Geochimica et Cosmochimica Acta 365 (2024) 53–69

Contents lists available at ScienceDirect

Geochimica et Cosmochimica Acta

journal homepage: www.elsevier.com/locate/gca

Zirconium stable isotope fractionation during intra-crustal magmatic differentiation in an active continental arc

Lisa J. Zieman [a,*], Mauricio Ibañez-Mejia [a], François L.H. Tissot [b], Hannah G.D. Tompkins [a], Natalia Pardo [c], Elias M. Bloch [d]

[a] Department of Geosciences, University of Arizona, Tucson, AZ 85721, USA
[b] The Isotoparium, Division of Geological and Planetary Sciences, California Institute of Technology, Pasadena, CA 91125, USA
[c] Department of Geosciences, University of Los Andes, Bogota, Colombia
[d] Institute of Earth Sciences, Université de Lausanne, Lausanne, Switzerland

ARTICLE INFO

Associate editor: Fangzhen Teng

Keywords:
Zr isotopes
Magmatic differentiation
Arclogite
Continental arc

ABSTRACT

Zirconium (Zr) stable isotope variations occur among co-existing Zr-rich accessory phases as well as at the bulk-rock scale, but the petrologic mechanism(s) responsible for Zr isotope fractionation during magmatic differentiation remain unclear. Juvenile magma generation and intra-crustal differentiation in convergent continental margins may play a crucial role in developing Zr isotope variations, and the Northern Volcanic Zone of the Andes is an ideal setting to test this hypothesis. To investigate the influence of these processes on Zr stable isotope compositions, we report $\delta^{94/90}Zr_{NIST}$ of whole rock samples from: 1) juvenile arc basalts from the Quaternary Granatifera Tuff, Colombia; 2) lower crust-derived garnet pyroxenites (i.e., arclogites), hornblendites, and gabbroic cumulates found in the same unit; and 3) felsic volcanic products from the Doña Juana Volcanic Complex, a dacitic composite volcano in close proximity to and partially covering the Granatifera Tuff. The basalts have $\delta^{94/90}Zr_{NIST}$ values ranging from -0.025 ± 0.018 ‰ to $+0.003 \pm 0.015$ ‰ (n = 8), within the range of mid-ocean ridge basalts. The dacites have $\delta^{94/90}Zr_{NIST}$ values ranging from $+0.008 \pm 0.013$ ‰ to $+0.043 \pm 0.015$ ‰ (n = 14), slightly positive relative to the Granatifera and mid-ocean ridge basalts. In contrast, the (ultra) mafic cumulates have highly variable, predominantly positive $\delta^{94/90}Zr_{NIST}$ values, ranging from -0.134 ± 0.012 ‰ to $+0.428 \pm 0.012$ ‰ (n = 15). Individual grains and mineral fractions of major rock-forming phases, including garnet (n = 21), amphibole (n = 9), and clinopyroxene (n = 18), were analyzed from 8 (ultra)mafic cumulates. The mineral fractions record highly variable Zr isotopic compositions, with inter-mineral fractionation ($\Delta^{94/90}Zr_{garnet\text{-}amphibole}$) up to 2.067 ‰. Recent *ab initio* calculations of Zr–O bond force constants in rock-forming phases predict limited inter-mineral Zr isotope fractionation in high-temperature environments, suggesting that the large fractionations we observe are not the product of vibrational equilibrium processes. Instead, we propose a scenario in which large Zr isotopic fractionations develop kinetically, induced by sub-solidus Zr diffusion between coexisting phases via changes in Zr distribution coefficients that arise from changes in temperature. Altogether, Zr isotope variability in this calc-alkaline continental arc setting exhibits no correlation with indices of magmatic differentiation (e.g., Mg#, SiO_2), and is not a simple function of fractional crystallization. Furthermore, the garnet clinopyroxenite cumulates studied here represent density-unstable lower arc crust material; consequently, material with isotopically variable $\delta^{94/90}Zr$ can be recycled into the mantle as a consequence of lower crustal foundering.

1. Introduction

Zirconium (Zr) is a high field strength element (HFSE) commonly used to study petrogenetic processes like magma differentiation, mantle melting, and crustal evolution (e.g., Münker et al., 2004; Weyer et al., 2003). Zirconium is also a major constituent of the mineral zircon ($ZrSiO_4$), a robust mineral used extensively for geochronology. Although Zr isotopes have been widely studied in extra-terrestrial materials for nucleosynthetic and radiogenic variations (e.g., Akram and Schönbächler, 2016; Schönbächler et al., 2002), mass-dependent

* Corresponding author.
E-mail address: lzieman@arizona.edu (L.J. Zieman).

https://doi.org/10.1016/j.gca.2023.11.023
Received 10 July 2023; Accepted 23 November 2023
Available online 29 November 2023

fractionations have only been explored in the last few years, and are receiving attention as a potential tracer of magmatic processes (e.g., Ibañez-Mejia and Tissot, 2019; Inglis et al., 2019). Interest in Zr isotopes comes in part from the fact that the geochemical behavior of Zr bears similarities to that of Ti, another HFSE that has been shown to undergo characteristic stable isotope fractionation during calc-alkaline vs. tholeiitic magmatic differentiation (Deng et al., 2019; Hoare et al., 2020; Johnson et al., 2019; Millet et al., 2016; Johnson et al., 2023), and is being exploited as a tracer of crustal evolution and differentiation through time (e.g., Greber et al., 2017; Saji et al., 2023). Thus, understanding how Zr stable isotopes behave during magmatic differentiation, particularly during calc-alkaline differentiation in thick magmatic arcs, has the potential to provide a new lens through which igneous differentiation processes can be studied.

The petrologic mechanism(s) driving Zr fractionation remain a matter of debate. Recent work has demonstrated that Zr stable isotopes vary in co-existing Zr-rich accessory phases, zircon and baddeleyite (Ibañez-Mejia and Tissot, 2019), as well as at the bulk-rock scale (Inglis et al., 2018; Inglis et al., 2019; Tian et al., 2020a). Positive $^{94/90}$Zr (i.e., $[(^{94}Zr/^{90}Zr)_{Sample}/(^{94}Zr/^{90}Zr)_{Standard} - 1]\cdot1000$) values have been documented for evolved igneous differentiates from the Hekla volcano, Iceland (Inglis et al., 2019) as well as several granitic reference materials (Tian et al., 2020a), and have been inferred to result from crystallization and removal of low $\delta^{94/90}$Zr zircon, which would drive residual magmas towards higher $\delta^{94/90}$Zr values. The isotopically 'light' nature of zircon growing in equilibrium with a silicate liquid has been predicted theoretically using *ab initio* calculations (Chen et al., 2020; Méheut et al., 2021) and demonstrated experimentally under controlled laboratory conditions (Tompkins et al., 2023). However, as recognized by several of these recent studies (Chen et al., 2020; Méheut et al., 2021; Tissot and Ibañez-Mejia, 2021) and demonstrated by Tompkins et al. (2023), the large range of natural variations observed in magmatic systems cannot be explained by equilibrium fractionation alone, and must instead be influenced –if not overwhelmingly controlled– by kinetic fractionation effects. For example, compositionally zoned zircon of calc-alkaline plutonic rocks from the Gangdese arc, Tibet (Guo et al., 2020), were shown by Tompkins et al. (2023) to exhibit a temperature-dependency that is inconsistent with equilibrium fractionation. Perhaps more striking are the zircon and baddeleyite results from an anorthositic gabbro from the Duluth Complex, Minnesota (FC-1), which show extreme fractionations (up to ~5 ‰) within a single rock that are arguably explained by the removal of isotopically heavy zircon from an evolving melt (Ibañez-Mejia and Tissot, 2019). Thus, differentiating between equilibrium vs. kinetic isotope fractionation effects in different geologic environments, both at low- and high-T, remains a key challenge in advancing our understanding of natural Zr isotope variations.

Despite numerous previous studies of Zr stable isotopes in magmatic environments (e.g., Guo et al., 2023; Guo et al., 2020; Ibañez-Mejia and Tissot, 2019; Tompkins et al., 2020; 2023; Yuan et al., 2022), how Zr stable isotopes fractionate (or not) during intra-crustal magmatic differentiation in continental arcs remains entirely unexplored. Furthermore, previous work has primarily focused on zircon-bearing rocks, but the behavior of Zr isotopes in mafic magmatic systems where Zr is primarily hosted in rock-forming phases rather than accessory phases such as zircon or baddeleyite, is also entirely unknown. In this study, we explore Zr isotope variations in the root of a continental magmatic system, which allows us to evaluate: 1) the effect that lower-crustal processes may have in fractionating Zr during magmatic differentiation in continental arcs, and 2) the occurrence of mass-dependent Zr isotope fractionation in the absence of Zr-rich accessory phases. In particular, we measured Zr isotopic compositions in 1) juvenile arc magmas, 2) lower crust-derived (ultra)mafic cumulates that crystallized from these magmas, 3) rock-forming mineral separates of these (ultra) mafic cumulates, and 4) evolved volcanic products erupted from a dacitic Pleistocene-Holocene composite volcano. All these samples belong to the same volcanic province in the Northern Volcanic Zone (NVZ) of the Andes, the Doña Juana/Animas/Mercaderes, thus allowing these different datasets to be interpreted cohesively. Finally, for the lower crustal cumulates, we present: i) Zr isotopic measurements for whole rocks as well as mineral fractions of garnet, clinopyroxene, and amphibole; and ii) inter-mineral distribution coefficients for elemental Zr partitioning (D_{Zr}) for a series of samples with well-determined peak temperatures, to investigate which phases and processes may be controlling the Zr budget and observed isotope fractionation in the lower crust of active continental arcs.

2. Samples and methods

2.1. Samples from the Andean Northern Volcanic Zone (NVZ)

The NVZ is the northernmost active volcanic segment of the Andes, extending from 5°N in central Colombia to 1°S in central Ecuador (Fig. 1a). Arc volcanism ceases to the north at the Bucaramanga flat slab and to the south at the Peruvian flat slab (e.g., Syracuse et al., 2016). On the western flank of the Colombian Central Cordillera at 1.5°N, a mafic ignimbrite-dominated volcanic succession, the Granatifera Tuff (GT), includes basalt to basaltic andesite volcanic bombs as well as (ultra) mafic intrusive lithic fragments that sample the lower crust and mantle (Fig. 1b). The GT is no older than 238 ka (Zieman et al., 2023), indicating it contains samples of the recent lower arc crust, sub-arc mantle, and juvenile arc magmas.

The Mercaderes xenoliths consist of garnet-rich gabbros, hornblendites, pyroxenites, and peridotites, described by Weber et al. (2002), Rodriguez-Vargas et al. (2005), Bloch et al. (2017) and Zieman et al. (2023). Equilibrium pressures and temperatures determined for the Mercaderes xenoliths indicate that the gabbros, hornblendites, and clinopyroxenites derived from the lower arc crust (1.2–2.2 GPa, 920–1280 °C) and the garnet peridotites and some pyroxenites from the convecting mantle wedge and from near-slab depths (2.9–4.1 GPa, 1140–1290 °C) (Bloch et al., 2017; Zieman et al., 2023). All xenolith samples studied here are garnet-rich gabbros, hornblendites, and clinopyroxenites exhumed from the lower arc crust, with the exception of two samples— one garnet clinopyroxenite interpreted by Bloch et al. (2017) to represent foundered arc crust material (MEMX5) and one garnet clinopyroxenite postulated to be of deep metasomatized mantle origin (MEMX6).

In addition to mafic bombs and (ultra)mafic xenoliths sampled from the GT, we also studied felsic volcanic rocks from the Doña Juana Volcanic Complex (DJVC; Fig. 1c). Volcanism related to the Doña Juana stratovolcano partially covers the Granatifera Tuff and has been active since ~1.1 Ma (Pardo et al., 2019). The coeval construction of the DJVC and the GT, and their co-location within the volcanic arc of the NVZ (Fig. 1a), supports the notion that these samples can be used in concert to study magmatic differentiation in this continental arc setting. The samples from the DJVC studied here were selected to be representative of the average stratovolcano eruptive products of polygenetic volcanoes found throughout the NVZ of the Andes (Bryant et al., 2006; Chiaradia et al., 2009).

2.2. Methods

Mafic bombs (n = 8), felsic extrusive volcanic samples (n = 14), and garnet pyroxenite (±amphibole) cumulates (n = 15) were ground to a fine powder using an alumina dish shatterbox. Major element concentrations were measured via XRF at Hamilton College. For Zr isotopes, aliquots of the same sample powders used for major and trace element geochemistry were digested via alkali flux fusion using an ultra-pure Li tetraborate flux (Alfa-Aesar 'puratronic') to ensure complete digestion of all rock-forming and any accessory phases. The known Zr blank of our flux is 3.5 ng/g, determined by isotope dilution. Samples were processed by mixing approximately 300 mg of sample powder with 600 mg of flux (1:2 sample to flux ratio) in ultra-pure graphite crucibles and fused at

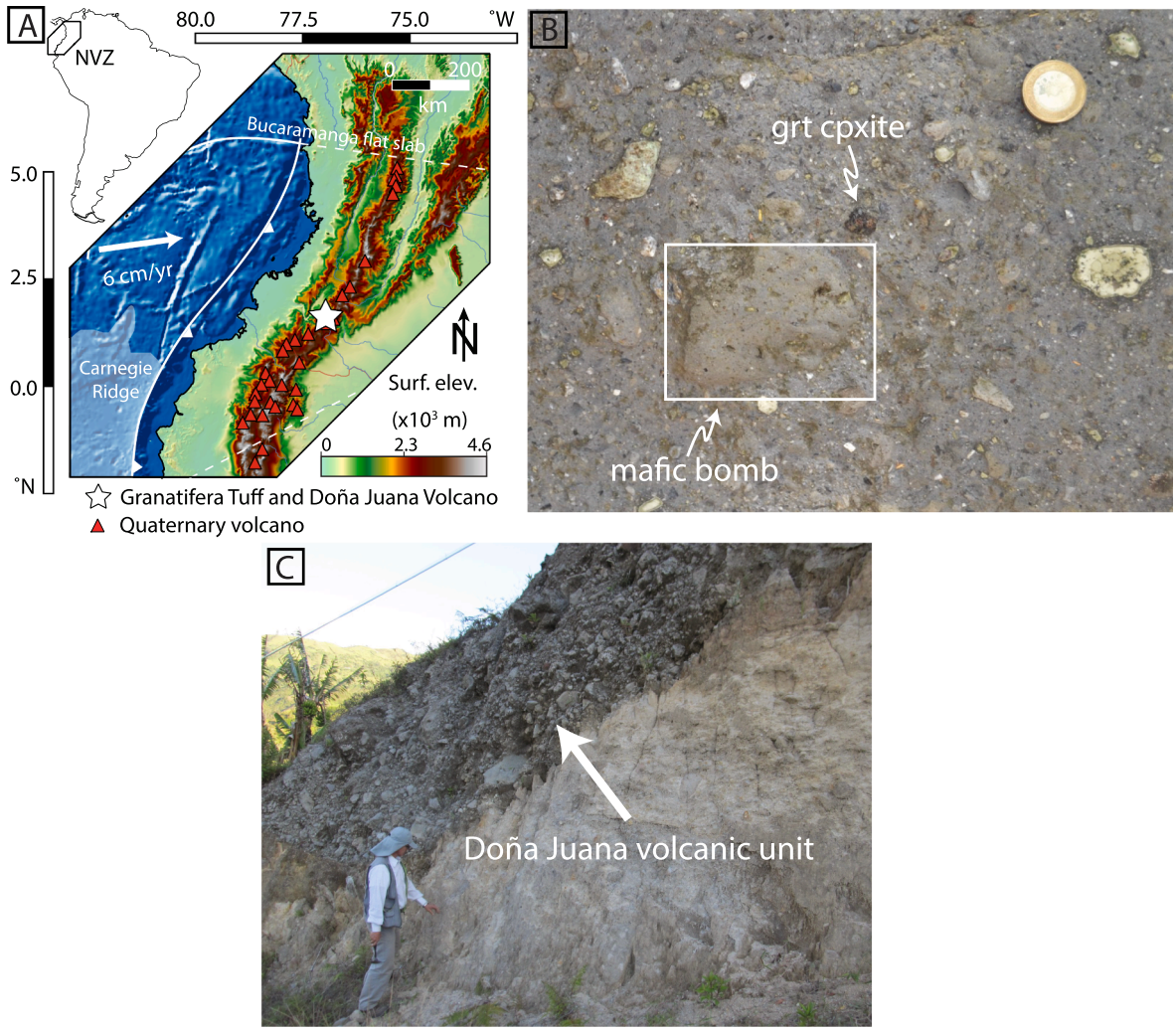

Fig. 1. A) Map of the Andean Northern Volcanic Zone (NVZ) showing the location of the Granatifera Tuff and the Doña Juana Volcanic Complex. B) Field photo of the Granatifera Tuff containing a garnet clinopyroxenite cumulate and a mafic bomb. C) Typical dacitic unit of the Doña Juana Volcanic Complex, the felsic volcanic rocks measured in this study.

1000 °C for 15 min. Fused beads were then crushed, and clean glass fragments (~100 mg) were picked with plastic tweezers under a binocular microscope to avoid graphite coating from the crucible. Known masses of glass were spiked with a ^{91}Zr-^{96}Zr double spike calibrated by Tompkins et al. (2020) to achieve an optimal 0.43:0.57 spike: sample Zr-mass ratio, and dissolved in 4 mL of 3 M HNO_3 + 0.5 M HF at 130 °C for 12 h. After full dissolution of the glass was confirmed by visual inspection, samples were dried, re-dissolved in 3 mL 3 M HNO3 + 0.4 M H_3BO_3, dried again to remove F^- by preferential evaporation of volatile BF_3 gas, and lastly re-dissolved in 10 mL 3 M HNO_3 for Zr purification by column chemistry.

Zirconium was purified using a four-step ion exchange chromatography procedure. These steps have been described in detail elsewhere (Ibañez-Mejia and Tissot, 2019; Tompkins et al., 2020, 2023; Klaver et al., 2021) and are only briefly summarized here. First, samples were run through 2 mL cartridges of Eichrom TODGA resin to remove most matrix elements, followed by a 'matrix cleanup' chemistry using 150 µl of Bio-Rad AG1-X8 resin in 6 cm-long columns to remove residual major elements (e.g., Fe, Cr, and Mg). Next, REE and Hf were removed using Eichrom Ln-Spec resin following the procedure detailed in Tompkins et al. (2020). The final Zr cut was run through Bio-Rad AG1-X8 resin, also described in Tompkins et al. (2020), to further remove any remaining Mo and Ru present in the samples, as isotopes of these two elements have direct isobaric interferences with Zr atomic masses. Purified Zr cuts were then dried, and residual organics from the resin were removed by oxidizing in 1 mL of 16 M HNO_3 and 1 mL of 30 % H_2O_2. Once dried again, samples were redigested in 1 mL concentrated HNO_3 and 1 mL concentrated HF to ensure all Zr was in solution. Finally, samples were dried to a small drop (to keep Zr in solution) and taken up in 0.59 M HNO_3 + 0.28 M HF for MC-ICP-MS measurement.

Pure garnet, clinopyroxene, and amphibole mineral separates were carefully hand-picked from 8 garnet clinopyroxenite and/or hornblendite cumulates under a binocular microscope, paying close attention to avoid inclusions. Three fractions weighing between 5 and 15 mg for each mineral per cumulate sample were leached in 10 mL 3 M HCl at 90 °C for 2 h to remove any surface contamination and/or phosphate phases, and rinsed thrice with 4 mL milli-Q water. The pre-cleaned fractions were then digested in a mixture of 3 mL concentrated HF and 1 mL concentrated HNO_3, heated for 12 h at 130 °C, dried, and re-digested in 4 mL aqua regia. After heating at 130 °C for over 36 h, the samples were again dried, re-dissolved in 3 mL HF and 1 mL concentrated HNO_3, fluxed for another 12 h, re-dried, and were finally digested in 4 mL of 3 M HNO_3 + 0.4 M boric acid. Samples were heated several hours to bring any residual fluorides back into solution, and then re-dried to volatilize residual F^- ions as BF_3 gas. A small aliquot (2.5 % of the total acid volume) of each sample was used to measure Ca, Fe, Mg, and Zr concentrations using an Agilent 7900 quadrupole ICP-MS at the University of Rochester to assess the purity of the mineral separates (see

discussion section). With the known Zr concentrations for each sample, solutions were then optimally spiked (Tompkins et al., 2020) with the ^{91}Zr-^{96}Zr double spike described above, heated for 12 h, dried, and re-digested in 1 mL concentrated HNO_3 to ensure equilibration between the spike and sample. Finally, samples were dried and dissolved in 3 M HNO_3 for Zr purification using the same four-step ion exchange chemistry described above.

Zr isotopic measurements were conducted using a Thermo Scientific Neptune Plus MC-ICP-MS equipped with an Aridus 3 at the Isotoparium (California Institute of Technology). Whole rock and mineral fraction samples diluted to ~45–65 ng/g of Zr were measured 2–4 times at a ^{90}Zr beam intensity of ~6–9 V with a sensitivity of ~420 V/ppm of total Zr. For more details on the mass spectrometry and double-spike data reduction methods see Tompkins et al. (2020). All data were reduced using both the '4-ratio minimization' and 'exact solving' approaches (Tompkins et al., 2020). Both reduction methods yield results that are

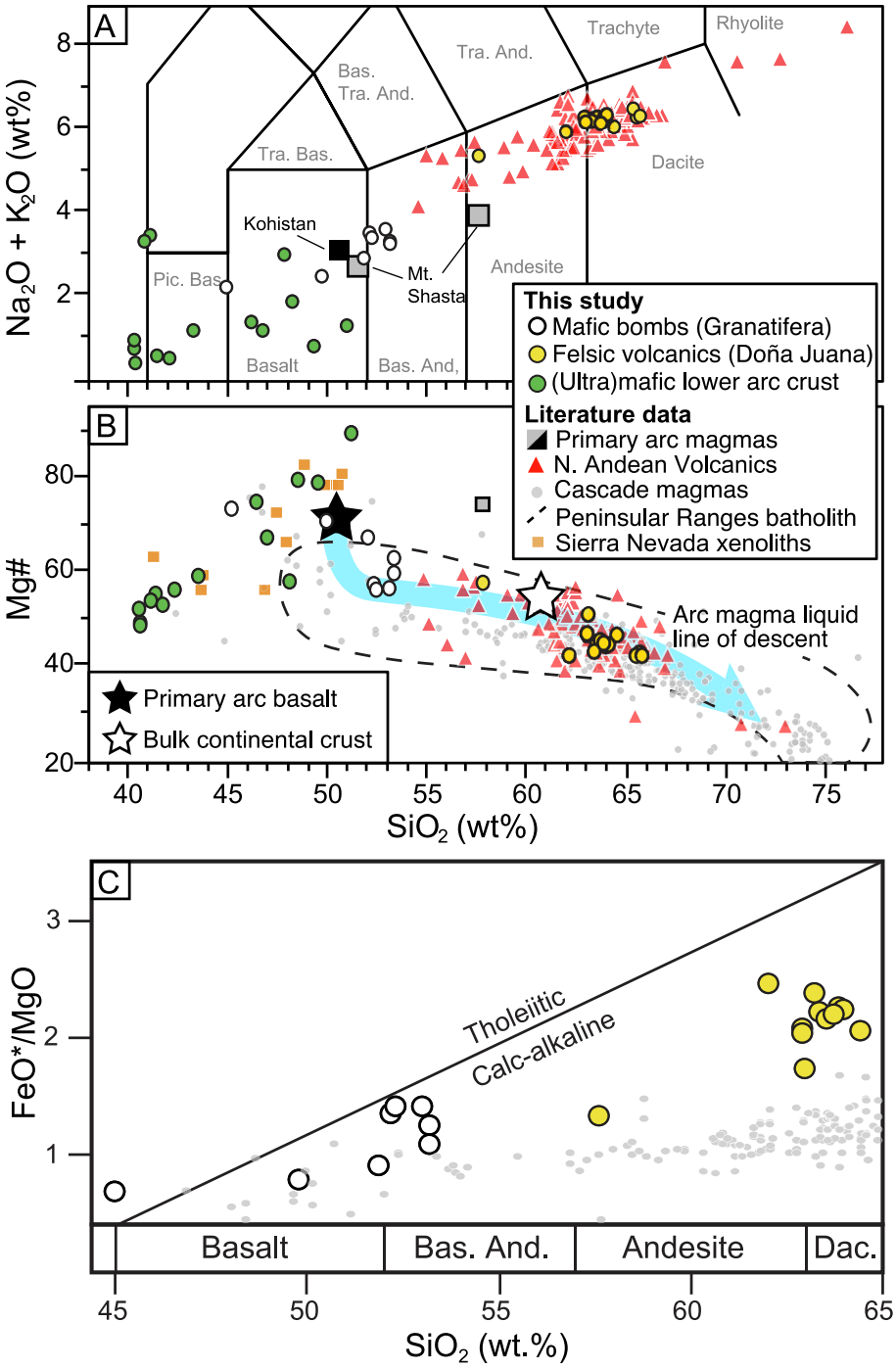

Fig. 2. Major element geochemistry of the NVZ whole rock volcanics and Mercaderes (ultra)mafic cumulates measured in this study. A) Total-alkali-silica classification. B) Mg# vs. SiO_2 wt.% showing the inferred liquid line of descent (blue arrow) from a primary arc basalt after Lee (2014). C) Calc-alkaline vs. tholeiitic discrimination diagram. Primary continental arc magmas are from Kohistan (Jagoutz, 2010) and the Cascades (Mt. Shasta; Baker et al., 1994). North Andean volcanics are from Bryant et al. (2006) and Chiaradia et al. (2009). Also plotted are continental arc-related rocks associated with the North American Cordillera including Cascade volcanics (Lee et al., 2006), Peninsular Ranges Batholith plutonic samples (Lee et al., 2007), and Sierra Nevada lower crustal garnet pyroxenite xenoliths (Lee et al., 2006). (For interpretation of the references to colour in this figure legend, the reader is referred to the web version of this article.)

undistinguishable within uncertainties. Zirconium isotopic results are reported throughout this study as $\delta^{94/90}$Zr per mil (‰) deviations from the NIST RM 8299 (Tissot et al., 2023), calculated as $\delta^{94/90}Zr = [(^{94/90}Zr_{sample}/^{94/90}Zr_{NIST}) - 1]*10^3$).

Zirconium concentrations in rock forming phases were measured in thin section by LA-ICP-MS at the Arizona LaserChron Center using a Thermo Element2 ICP-MS connected to a Teledyne Iridia laser. The spot size was set to 110 μm, shot count to 320, and frequency to 8 Hz. The total lasing time for each spot was 40 s. Six to 8 groups of adjacent garnet, clinopyroxene, and/or amphibole grains were analyzed, measuring 2–3 points per grain. The data were reduced with Iolite Version 2.3 software using BCR2G as the primary reference material and Mg as the internal standard for normalization. Magnesium concentrations for all phases were determined from electron microprobe analyses by Zieman et al. (2023) and Bloch et al. (2017).

3. Results

3.1. Major element geochemistry of studied samples

Results of major element geochemical analyses for the studied samples are shown in Fig. 2, and data are reported in the Supplementary Materials (Table S1). The mafic bombs from the GT are classified as basalts to basaltic andesites on a total-alkali-silica diagram (TAS; Fig. 2a), and their Mg# (56–73) and SiO_2 contents indicate they represent near-primary arc magmas (Fig. 2b). The DJVC felsic volcanics are andesites to dacites on the TAS diagram and representative of the typical range of compositions defined by other Quaternary volcanic centers in the NVZ (Fig. 2). Both the mafic bombs and felsic extrusives are calc-alkaline (Fig. 2c) and fall within the liquid line of descent of evolved residual liquids formed during calc-alkaline differentiation (Fig. 2b; Lee et al., 2006; Lee et al., 2007; Müntener and Ulmer, 2018). They plot within the range of volcanics from the Cascades and plutonic samples from the Peninsular Ranges batholiths, evolved arc-related

Table 1
Zirconium isotopic composition of Mercaderes and Doña Juana whole rock samples.

Sample ID	n	Zr_{Spk}/Zr_{Tot}*	Zr stable isotope compositions§						Mo interference	
			$\delta^{91/90}$Zr	±2σ	$\delta^{94/90}$Zr	±2σ	$\delta^{96/90}$Zr	±2σ	$^{98}Mo/^{90}Zr$†	Mo/Zr††
Felsic volcanics										
DJV1	4	46 %	0.003	*0.003*	0.012	*0.009*	0.017	*0.015*	1.50E-05	0.002 %
DJV2	4	43 %	0.003	*0.003*	0.010	*0.009*	0.015	*0.015*	1.70E-05	0.002 %
DJV3	4	38 %	−0.024	*0.005*	−0.093	*0.018*	−0.142	*0.026*	1.48E-05	0.002 %
DJV4	4	46 %	0.006	*0.005*	0.025	*0.018*	0.031	*0.026*	2.08E-05	0.003 %
DJV5	4	44 %	0.009	*0.005*	0.036	*0.018*	0.049	*0.026*	1.53E-05	0.002 %
DJV6	4	46 %	0.010	*0.004*	0.043	*0.015*	0.057	*0.022*	1.25E-05	0.002 %
DJV7	4	45 %	0.006	*0.004*	0.025	*0.015*	0.035	*0.022*	1.56E-05	0.002 %
DJV8	4	47 %	0.010	*0.004*	0.040	*0.015*	0.055	*0.022*	1.76E-05	0.002 %
DJV9	4	40 %	0.005	*0.004*	0.018	*0.015*	0.029	*0.022*	1.37E-05	0.002 %
DJV10	4	43 %	0.008	*0.004*	0.036	*0.015*	0.048	*0.022*	1.62E-05	0.002 %
DJV11	4	42 %	0.002	*0.004*	0.010	*0.015*	0.012	*0.022*	9.23E-05	0.012 %
DJV12	4	44 %	0.009	*0.004*	0.038	*0.015*	0.052	*0.022*	1.50E-05	0.002 %
DJV13	4	44 %	0.004	*0.003*	0.018	*0.013*	0.022	*0.018*	2.20E-04	0.028 %
DJV14	4	40 %	0.003	*0.003*	0.011	*0.013*	0.019	*0.018*	1.89E-05	0.003 %
DJV1 repeat	4	47 %	0.002	*0.003*	0.008	*0.013*	0.010	*0.018*	2.17E-05	0.003 %
Granatifera mafic magmatic bombs										
MXLB01	4	43 %	0.001	*0.004*	0.003	*0.015*	0.004	*0.022*	1.48E-05	0.002 %
MXLB02	4	45 %	−0.003	*0.004*	−0.011	*0.015*	−0.020	*0.022*	2.27E-05	0.003 %
MXLB03	4	44 %	−0.004	*0.004*	−0.010	*0.015*	−0.024	*0.022*	1.82E-05	0.002 %
MXLB04	4	42 %	−0.002	*0.003*	−0.002	*0.009*	−0.011	*0.015*	1.90E-05	0.002 %
MXLB07	7	42 %	−0.002	*0.002*	−0.006	*0.008*	−0.010	*0.013*	2.07E-05	0.003 %
MXLB08	4	44 %	−0.001	*0.005*	−0.002	*0.018*	−0.010	*0.026*	1.97E-05	0.003 %
MXLB15	4	44 %	0.000	*0.005*	0.000	*0.018*	−0.003	*0.026*	1.57E-05	0.002 %
MXLB17	4	43 %	−0.007	*0.005*	−0.025	*0.018*	−0.040	*0.026*	2.53E-05	0.003 %
Garnet (±amphibole) clinopyroxenite cumulates										
MEMX1	7	45 %	−0.033	*0.002*	−0.126	*0.009*	−0.191	*0.014*	1.64E-05	0.002 %
MEMX2	4	43 %	−0.020	*0.003*	−0.075	*0.013*	−0.116	*0.018*	2.74E-05	0.004 %
MEMX3	4	45 %	0.001	*0.003*	0.007	*0.013*	0.002	*0.018*	1.49E-05	0.002 %
MEMX4	4	39 %	−0.009	*0.003*	−0.039	*0.012*	−0.054	*0.018*	4.82E-05	0.007 %
MEMX5	4	35 %	0.027	*0.003*	0.101	*0.012*	0.162	*0.018*	4.77E-05	0.007 %
MEMX6	4	43 %	−0.034	*0.003*	−0.134	*0.012*	−0.198	*0.018*	3.56E-05	0.005 %
MEMX7	4	40 %	0.108	*0.003*	0.428	*0.012*	0.633	*0.018*	2.35E-05	0.003 %
MMXA02	4	46 %	0.000	*0.003*	0.005	*0.011*	0.002	*0.015*	2.09E-05	0.003 %
MMXA09	4	48 %	0.001	*0.003*	0.008	*0.011*	0.008	*0.015*	1.09E-05	0.001 %
MMXG02	7	52 %	0.025	*0.002*	0.103	*0.009*	0.146	*0.013*	1.70E-05	0.002 %
MMXG04	4	49 %	0.085	*0.003*	0.341	*0.011*	0.497	*0.015*	1.06E-05	0.001 %
MMXG07	7	49 %	0.010	*0.002*	0.046	*0.009*	0.058	*0.013*	1.35E-05	0.002 %
MMXP02	4	43 %	−0.018	*0.003*	−0.071	*0.011*	−0.107	*0.015*	1.42E-05	0.002 %
MMXP05	4	48 %	−0.012	*0.003*	−0.047	*0.012*	−0.074	*0.019*	8.85E-06	0.001 %
MMXP08	4	49 %	0.038	*0.003*	0.152	*0.012*	0.222	*0.019*	2.74E-05	0.003 %

*Fraction of Zr (by mass) from double spike in the spike-sample mixture, calculated by isotope dilution
§Reported values are means of all measured replicates for each fraction, expressed as part per million deviations relative to the Zr-NIST standard according to: $\delta^{9X/90}Zr = ([^{9X/90}Zr]_{Sample}/[^{9X/90}Zr]_{NIST} - 1) * 10^6$.
Uncertainties reported for each sample are 2SE, calculated using the daily external reproducibility of the NIST standard (2SD) divided by the square root of the number of replicates measured.
(i.e., $2SE = 2SD_{External}/\sqrt{n}$).
†Ratio of measured ion beam intensities.
††Percent Mo/Zr (atomic).

rocks from the North American Cordillera. Thus, our volcanic samples represent near-primary arc magmas (GT bombs) and evolved residual melts (DJVC volcanics) typical of continental arcs.

The lower crust-derived gabbro, hornblendite, and clinopyroxenite xenoliths have low alkali and SiO_2 contents (<52 wt%). Their major element geochemistry overlaps with the lower crustal garnet pyroxenite xenoliths from the Mesozoic Sierra Nevada arc (Lee et al., 2006), supporting that they are representative of (ultra)mafic continental arc root cumulates. Thus, our lower crustal cumulates, in addition to our volcanic samples, are typical products of intra-crustal continental arc differentiation beyond the north Andean arc.

3.2. Zr isotopic compositions of NVZ mafic and felsic volcanic rocks

Zirconium isotope data for the GT mafic bombs and DJVC extrusives are reported in Table 1 and shown graphically in Fig. 3. The mafic bombs have near-zero $\delta^{94/90}$Zr values, ranging from −0.025 ± 0.018 ‰ to +0.003 ± 0.015 ‰. These results are within the range of mid-ocean ridge basalts (MORBs) reported by Inglis et al. (2019), recalculated using $\delta^{94/90}Zr_{NIST} = \delta^{94/90}Zr_{IPGP} + 0.056 \pm 0.002$ (Tissot et al., 2023), which are shown as a gray band in Fig. 3. The $\delta^{94/90}$Zr values of the DJVC felsic volcanics are predominantly slightly positive relative to the GT mafic bombs and MORBs, ranging from 0.008 ± 0.013 ‰ to 0.043 ± 0.015 ‰. The only exception is sample DJV3 which is characterized by a $\delta^{94/90}$Zr value of −0.093 ± 0.018 ‰. Zirconium isotopic compositions of these mafic and felsic extrusive rocks do not correlate with SiO_2 wt. % or Mg #, indices for differentiation (Fig. 3).

3.3. Zr isotopic compositions of Mercaderes (ultra)mafic cumulates

Whereas the mafic and felsic volcanics exhibit a limited range of $\delta^{94/90}$Zr values, the lower crustal gabbroic, hornblendite, and clinopyroxenite cumulates display much greater variability. $\delta^{94/90}$Zr values of the whole rock cumulates are both negative and positive, with values ranging from −0.134 ± 0.012 ‰ to +0.428 ± 0.012 ‰ (Table 1) and heavy values being predominant over light ones. The major element chemistry of dissolved garnet, amphibole, and clinopyroxene mineral fractions from these cumulates, determined via solution ICPMS prior to spiking, is in excellent agreement with the electron microprobe mineral chemistry obtained by Bloch et al. (2017) and Zieman et al. (2023) for each of the studied samples (Fig. 4). This confirms the purity of digested separates for each phase. In terms of $\delta^{94/90}$Zr, the mineral fractions yielded even more fractionated and variable values compared to the bulk rocks (Fig. 5 and Fig. 6; Table 2) ranging from –0.836 ± 0.024 to +1.746 ± 0.021 ‰ (Table 1). In five of the eight cumulate samples studied, garnet is heavy relative to the whole rock and co-existing mineral phases (amphibole and/or clinopyroxene), whereas in two samples different aliquots are heavy and light, and in one sample all analyzed garnet fractions are light. No clear relationship is observed between $\delta^{94/90}$Zr and mineral chemistry (Fig. 7). The most extreme Zr isotopic compositions observed throughout this study are for garnet fractions from a garnet clinopyroxene hornblendite cumulate (MEMX1). The garnet mineral fractions from MEMX1 have $\delta^{94/90}$Zr values up to +1.746 ± 0.021 ‰ and co-existing amphibole fractions as low as −0.321 ± 0.014 ‰, resulting in the largest inter-mineral Zr isotope fractionation measured within an individual sample in this study ($\Delta^{94/90}Zr_{garnet\text{-}amphibole} = 2.067$ ‰).

3.4. In situ Zr concentrations in rock-forming phases

Zr concentrations [Zr] in amphibole, garnet, and clinopyroxene determined in thin sections via LA-ICP-MS are plotted in Fig. 8 for samples analyzed for Zr isotopes as well as additional garnet clinopyroxenite (±amphibole) cumulates from this same locality equilibrated within a wide range of temperatures (782–1280 °C; Bloch et al., 2017; Zieman et al., 2023). Zr concentrations range from 21 to 67 μg/g in amphibole, 2 to 50 μg/g in garnet, and 5 to 96 μg/g in clinopyroxene. With the exception of two samples (MEMX5 and MEMX6), [Zr] in clinopyroxene is always greater than [Zr] in garnet for each given sample (Fig. 8). When amphibole is present in the lower temperature samples (<1021 °C), [Zr] in amphibole falls between co-existing clinopyroxene and garnet. The majority of the samples exhibit significant variability in [Zr] for each given phase indicating that [Zr] in most minerals and samples studied here are not in equilibrium at the thin section or even at the hundreds of μm scale. Intra-crystalline [Zr] zoning in individual rock forming minerals could not be spatially resolved using our methods given the small grain sizes of the samples relative to the diameter of the

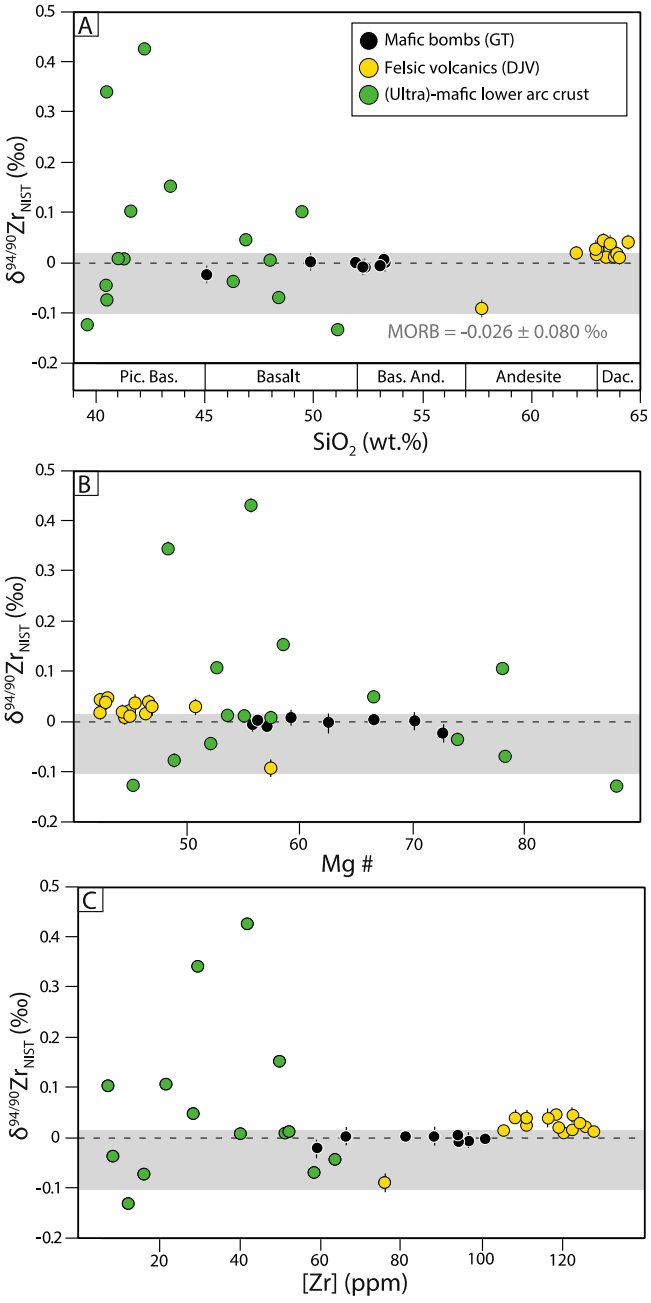

Fig. 3. Whole rock Zr isotopic composition ($\delta^{94/90}Zr = [(^{94/90}Zr_{sample}/^{94/90}Zr_{NIST})\text{-}1]*10^3$) vs. A) SiO_2 wt. %, B) Mg#, and C) [Zr] for mafic and felsic extrusive volcanic rocks as well as garnet clinopyroxenite (±amphibole) cumulates. Error bars are smaller than symbols where not visible, see Table 1. Range of MORBs (gray field) is from Inglis et al. (2019), recalculated relative to the NIST standard from the IPGP-Zr standard (IPGP-Zr $\delta^{94/90}Zr_{NIST} = -0.055 \pm 0.002$ ‰; Klaver et al., 2021).

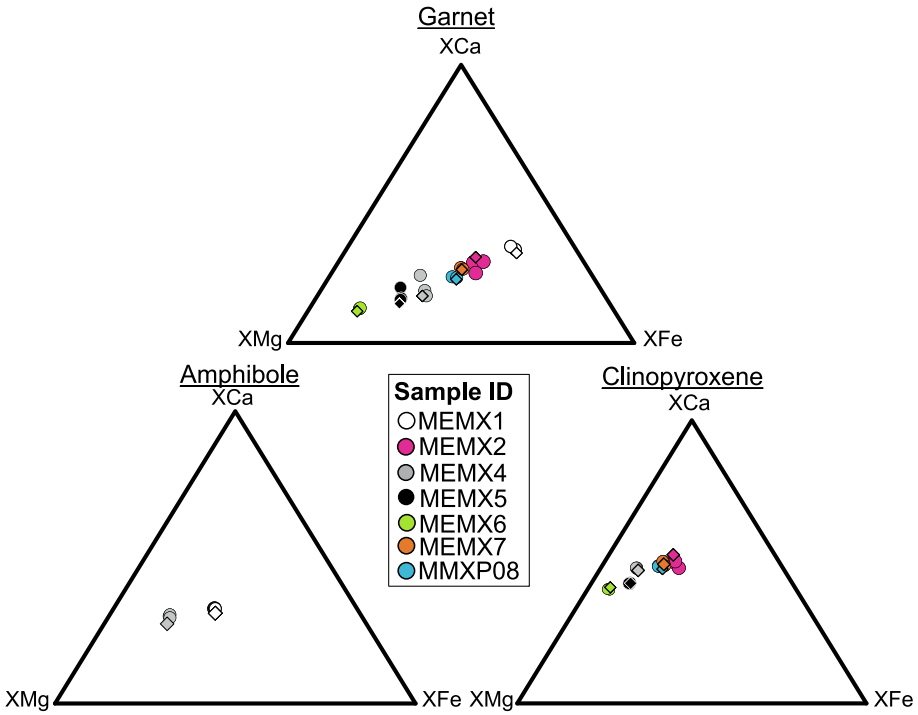

Fig. 4. Mole fraction chemistry of Ca, Mg, and Fe for the mineral fraction solutions that were analyzed for Zr isotopes (circles) compared to *in situ* mineral chemistry obtained by electron microprobe (diamonds) from Bloch et al. (2017).

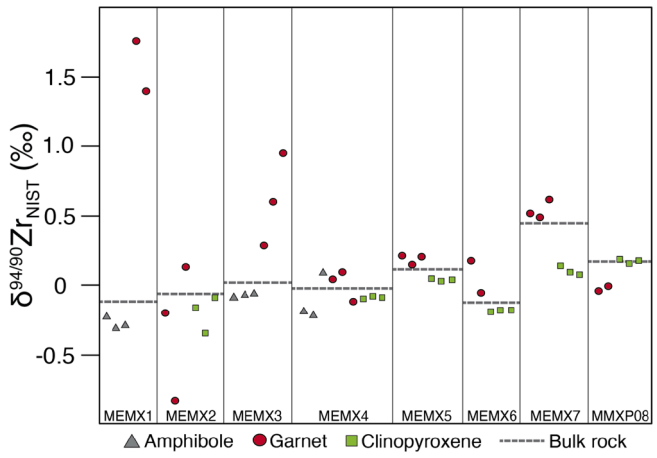

Fig. 5. Zirconium isotopic composition of garnet, clinopyroxene, and amphibole mineral fractions from the Mercaderes cumulates. Error bars are within symbol size.

laser ablation spot. For samples MEMX5 and MEMX6 which equilibrated at mantle conditions, [Zr] in clinopyroxene and garnet are more homogenous throughout the sample relative to the lower pressure (arc lithosphere) samples.

4. Discussion

4.1. Zr stable isotope fractionation during continental arc magma differentiation

Zr isotopic variability in continental arcs has not been previously studied. The compositional range covered by our samples, which include primitive basalts, lower crustal cumulates, and differentiated liquids produced by fractional removal of cumular assemblages (Bloch et al., 2017; Zieman et al., 2023), allows us to evaluate how crystal-liquid separation in the lower arc crust may influence the $\delta^{94/90}$Zr of Andean-type continental arcs and thus the continental crust.

The range of $\delta^{94/90}$Zr values observed in the GT's basaltic bombs is extremely limited, and the samples we studied have $\delta^{94/90}$Zr that are not only indistinguishable between one another within analytical uncertainty but also undistinguishable from the values determined for MORB (Fig. 3; Inglis et al., 2019). Therefore, these results indicate that hydrous partial melting of the sub-arc mantle in subduction zones does not induce resolvable fractionation of Zr isotopes relative to anhydrous melting. The similarity between our arc basalts and MORB also indicate that, at least in this section of the Andean arc, mass transfer from subducted components to the mantle wedge (e.g., through slab dehydration fluids) did not significantly influence the $\delta^{94/90}$Zr of primary arc basalts.

The Doña Juana volcanic rocks also show limited variability in $\delta^{94/90}$Zr. Most studied samples have slightly positive $\delta^{94/90}$Zr with respect to MORB and the GT mafic bombs. The most SiO_2-poor DJVC sample we studied is the sole exception, with a negative $\delta^{94/90}$Zr value of –0.093 ± 0.018 ‰ (not included in the mean value). Although the Zr variability is limited in the felsic volcanic rocks, there are resolvable sample-to-sample differences and a slight increase in $\delta^{94/90}$Zr with differentiation is observed. This is in contrast to the uniform Zr isotope composition of the mafic bombs. This difference in the DJVC felsic volcanics cannot be explained by crystallization of zircon because zircon-saturation was not achieved for the felsic volcanic rocks (see Fig. S1 in the Supplementary Material). On the other hand, this difference could be explained by crystallization of ilmenite, which is present in many of the lower crustal cumulates and is a phase expected to crystallize during calc-alkaline differentiation. *Ab initio* calculations predict that ilmenite should preferentially incorporate light Zr isotopes during equilibrium crystallization (Chen et al., 2020), which would drive evolved residual liquids to heavier Zr isotopic compositions, as observed in the Doña Juana dacitic volcanic rocks. If roughly 0.2 mass fraction of the total Zr were removed by ilmenite as a Rayleigh process during differentiation to produce the DJVC volcanics, the $\delta^{94/90}$Zr value of the magma would increase from the average composition of our basalts (-0.007 ‰) to a $\delta^{94/90}$Zr value of + 0.026 ‰ in the residual liquid. Given that Zr partition

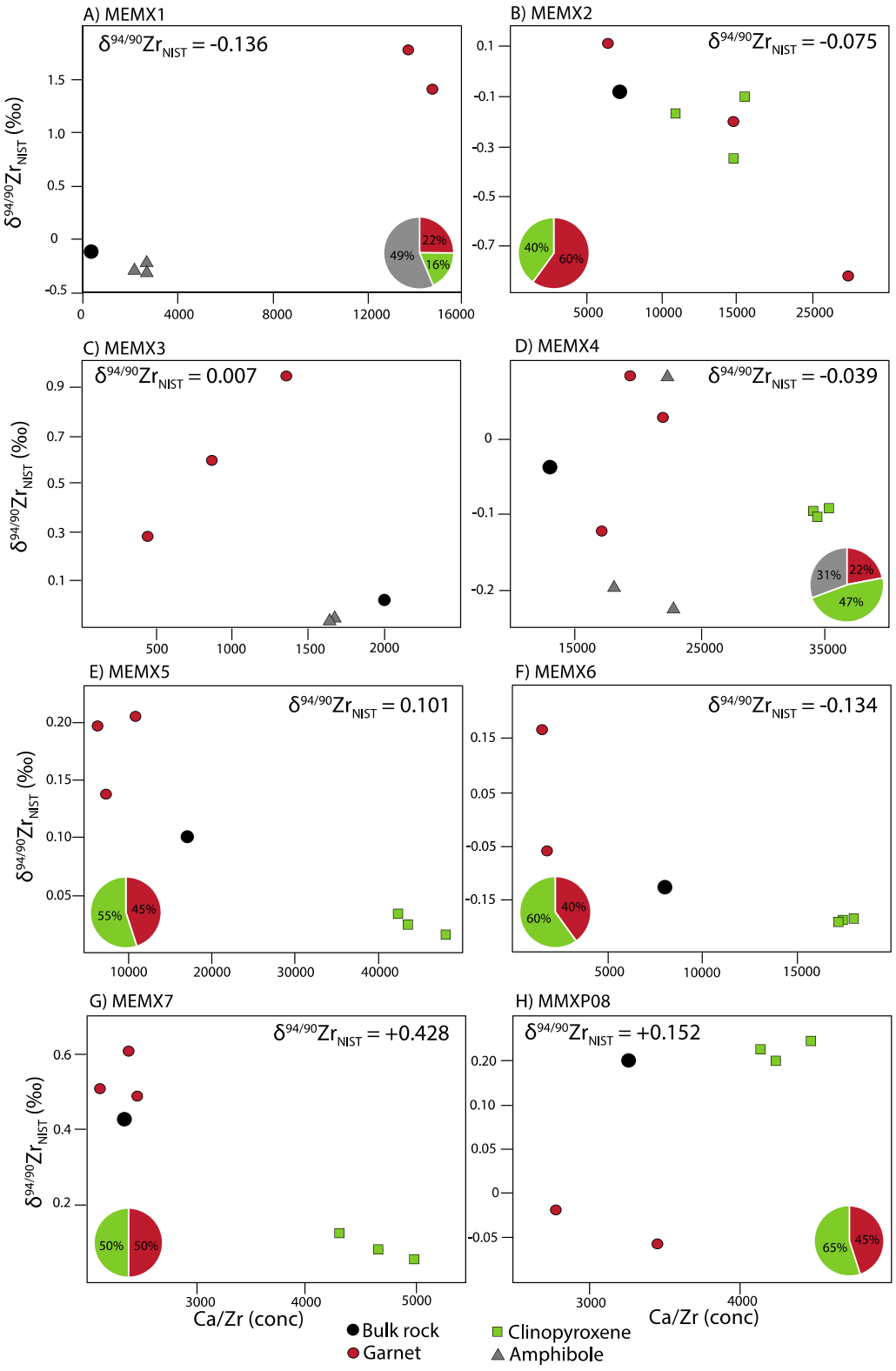

Fig. 6. Zirconium isotopic compositions of bulk rock and mineral fractions from eight garnet clinopyroxenite (±amphibole) cumulates vs. Ca/Zr ratios. Ca was chosen for the numerator because this is a major element that varies significantly between garnet, clinopyroxene, and amphibole, and Zr was chosen in the numerator to evaluate if the $\delta^{94/90}$Zr variations in each sample can be explained by simple two- or three-component mixing. Pie chart insets represent the modal abundances of major phases. Insets of $\delta^{94/90}$Zr values indicate the bulk rock isotopic compositions.

Table 2
Zirconium isotopic composition of minerals from (ultra)mafic lower crustal xenoliths.

Sample ID	n	Zr_{Spk}/Zr_{Tot}*	$\delta^{91/90}Zr$	±2σ	$\delta^{94/90}Zr$	±2σ	$\delta^{96/90}Zr$	±2σ	$^{98}Mo/^{90}Zr$†	Mo/Zr††
MEMX1: 22 % garnet, 16 % clinopyroxene, 49 % amphibole										
MEMX1 amph1	3	39 %	−0.060	*0.005*	−0.237	*0.018*	−0.352	*0.026*	3.29E-04	0.045 %
MEMX1 amph2	4	39 %	−0.082	*0.004*	−0.321	*0.014*	−0.477	*0.021*	2.65E-04	0.037 %
MEMX1 amph3	3	38 %	−0.078	*0.005*	−0.306	*0.020*	−0.454	*0.030*	5.73E-04	0.080 %
MEMX1 grt2	4	35 %	0.444	*0.005*	1.746	*0.021*	2.592	*0.032*	1.38E-03	0.201 %
MEMX1 grt3	2	33 %	0.351	*0.005*	1.382	*0.021*	2.053	*0.032*	3.74E-04	0.056 %
MEMX2: 60 % garnet, 40 % clinopyroxene										
MEMX2 grt1	3	31 %	−0.052	*0.005*	−0.206	*0.019*	−0.305	*0.028*	3.35E-04	0.051 %
MEMX2 grt2	1	28 %	−0.213	*0.006*	−0.836	*0.024*	−1.240	*0.036*	5.63E-04	0.090 %
MEMX2 grt3	3	35 %	0.030	*0.005*	0.118	*0.019*	0.175	*0.028*	1.80E-04	0.026 %
MEMX2 px1	4	34 %	−0.043	*0.004*	−0.170	*0.016*	−0.252	*0.024*	1.34E-04	0.020 %
MEMX2 px2	3	34 %	−0.090	*0.005*	−0.355	*0.019*	−0.527	*0.028*	2.00E-04	0.030 %
MEMX2 px3	3	34 %	−0.026	*0.005*	−0.103	*0.019*	−0.154	*0.028*	2.39E-04	0.035 %
MEMX3										
MEMX3 amph1	3	40 %	−0.023	*0.004*	−0.092	*0.016*	−0.137	*0.024*	1.56E-04	0.021 %
MEMX3 amph2	3	40 %	−0.022	*0.004*	−0.086	*0.016*	−0.128	*0.024*	1.87E-04	0.026 %
MEMX3 amph3	3	40 %	−0.019	*0.004*	−0.075	*0.016*	−0.112	*0.024*	8.48E-05	0.012 %
MEMX3 grt1	3	44 %	0.070	*0.004*	0.274	*0.016*	0.407	*0.024*	4.58E-05	0.006 %
MEMX3 grt2	3	42 %	0.148	*0.004*	0.581	*0.016*	0.863	*0.024*	3.85E-05	0.005 %
MEMX3 grt3	3	42 %	0.238	*0.004*	0.938	*0.016*	1.392	*0.024*	1.52E-04	0.020 %
MEMX4: 22 % garnet, 47 % clinopyroxene, 31 % amphibole										
MEMX4 amph1	2	30 %	−0.050	*0.005*	−0.197	*0.021*	−0.293	*0.031*	1.75E-04	0.027 %
MEMX4 amph2	2	29 %	−0.058	*0.006*	−0.227	*0.024*	−0.337	*0.036*	4.95E-04	0.077 %
MEMX4 amph3	2	25 %	0.021	*0.005*	0.081	*0.019*	0.120	*0.029*	6.03E-04	0.099 %
MEMX4 grt1	1	20 %	0.006	*0.006*	0.025	*0.024*	0.038	*0.036*	3.97E-04	0.069 %
MEMX4 grt2	1	23 %	0.021	*0.006*	0.082	*0.024*	0.121	*0.036*	4.04E-04	0.068 %
MEMX4 grt3	1	23 %	−0.033	*0.006*	−0.128	*0.024*	−0.191	*0.036*	1.14E-04	0.019 %
MEMX4 px1	2	31 %	−0.027	*0.005*	−0.107	*0.021*	−0.159	*0.031*	6.66E-04	0.102 %
MEMX4 px2	2	30 %	−0.024	*0.006*	−0.095	*0.024*	−0.141	*0.036*	6.19E-04	0.096 %
MEMX4 px3	3	31 %	−0.025	*0.005*	−0.099	*0.019*	−0.147	*0.028*	4.06E-04	0.062 %
MEMX5: 45 % garnet, 55 % clinopyroxene										
MEMX5 grt1	2	29 %	0.052	*0.005*	0.203	*0.021*	0.301	*0.031*	2.29E-04	0.036 %
MEMX5 grt2	2	31 %	0.035	*0.005*	0.136	*0.021*	0.202	*0.031*	2.89E-04	0.044 %
MEMX5 grt3	3	30 %	0.049	*0.004*	0.194	*0.016*	0.288	*0.024*	3.49E-04	0.054 %
MEMX5 px1	2	32 %	0.008	*0.005*	0.032	*0.021*	0.048	*0.031*	5.56E-04	0.084 %
MEMX5 px2	2	28 %	0.004	*0.005*	0.015	*0.019*	0.023	*0.029*	5.15E-04	0.082 %
MEMX5 px3	2	31 %	0.006	*0.005*	0.024	*0.021*	0.035	*0.031*	2.93E-04	0.045 %
MEMX6: 40 % garnet, 60 % clinopyroxene										
MEMX6 grt1	2	37 %	0.042	*0.005*	0.166	*0.019*	0.247	*0.028*	4.29E-04	0.060 %
MEMX6 grt3	3	40 %	−0.016	*0.004*	−0.061	*0.015*	−0.091	*0.022*	1.31E-04	0.018 %
MEMX6 px1	3	39 %	−0.050	*0.005*	−0.197	*0.018*	−0.293	*0.026*	2.87E-04	0.040 %
MEMX6 px2	2	39 %	−0.049	*0.006*	−0.191	*0.022*	−0.283	*0.032*	4.77E-04	0.065 %
MEMX6 px3	3	38 %	−0.050	*0.005*	−0.196	*0.018*	−0.290	*0.026*	1.90E-04	0.026 %
MEMX7: 50 % garnet, 50 % clinopyroxene										
MEMX7 grt1	3	38 %	0.128	*0.005*	0.503	*0.020*	0.746	*0.030*	6.73E-04	0.094 %
MEMX7 grt2	2	37 %	0.122	*0.005*	0.479	*0.021*	0.712	*0.032*	2.99E-04	0.042 %
MEMX7 grt3	2	41 %	0.152	*0.006*	0.600	*0.022*	0.890	*0.032*	2.37E-04	0.032 %
MEMX7 px1	3	42 %	0.032	*0.005*	0.126	*0.020*	0.186	*0.030*	5.59E-04	0.073 %
MEMX7 px2	3	39 %	0.021	*0.005*	0.084	*0.020*	0.125	*0.030*	4.41E-04	0.061 %
MEMX7 px3	3	31 %	0.016	*0.005*	0.063	*0.020*	0.094	*0.030*	4.69E-04	0.072 %
MMXP08: 45 % garnet, 55 % clinopyroxene										
MMXP08 grt1	4	33 %	−0.014	*0.005*	−0.057	*0.021*	−0.084	*0.032*	2.09E-03	0.314 %
MMXP08 grt2	3	38 %	−0.005	*0.004*	−0.020	*0.016*	−0.030	*0.024*	5.37E-04	0.075 %
MMXP08 px1	3	39 %	0.044	*0.004*	0.173	*0.016*	0.257	*0.024*	8.73E-04	0.121 %
MMXP08 px2	3	37 %	0.038	*0.004*	0.148	*0.016*	0.220	*0.024*	2.85E-03	0.405 %
MMXP08 px3	2	36 %	0.041	*0.005*	0.163	*0.021*	0.242	*0.032*	1.96E-04	0.028 %

* Fraction of Zr (by mass) from double spike in the spike-sample mixture, calculated by isotope dilution

§ Reported values are means of all measured replicates for each fraction, expressed as part per million deviations relative to the Zr-NIST standard according to: $\delta^{9X/90}Zr = ([^{9X/90}Zr]_{Sample}/[^{9X/90}Zr]_{NIST} - 1) * 10^6$.

Uncertainties reported for each sample are 2SE, calculated using the daily external reproducibility of the NIST standard (2SD) divided by the square root of the number of replicates measured.

(i.e., $2SE = 2SD_{External}/\sqrt{n}$).

† Ratio of measured ion beam intensities.

†† Percent Mo/Zr (atomic).

Amph – amphibole. Grt – garnet. Cpx – clinopyroxene.

coefficients between ilmenite and silicate liquids range from approximately 0.6 to 0.8 (Klemme et al., 2006), moderate fractional removal of Zr by ilmenite is likely during calc-alkaline differentiation and not incompatible with the general increase in [Zr] of derivative liquids (because $D_{Zr} < 1$). Therefore, although the exact differentiation history of the DJVC extrusives is not well known, we suggest that the moderate increase in $\delta^{94/90}Zr$ between our primitive arc basalts and felsic volcanics is most likely due to ilmenite fractionation.

Altogether, the volcanic rocks studied here span a broad range of SiO_2 wt. % and Mg #, from basalts to dacites, and are representative of an evolving calc-alkaline differentiation sequence (Fig. 2). Thus, the limited Zr isotope variability observed in these samples indicates Zr

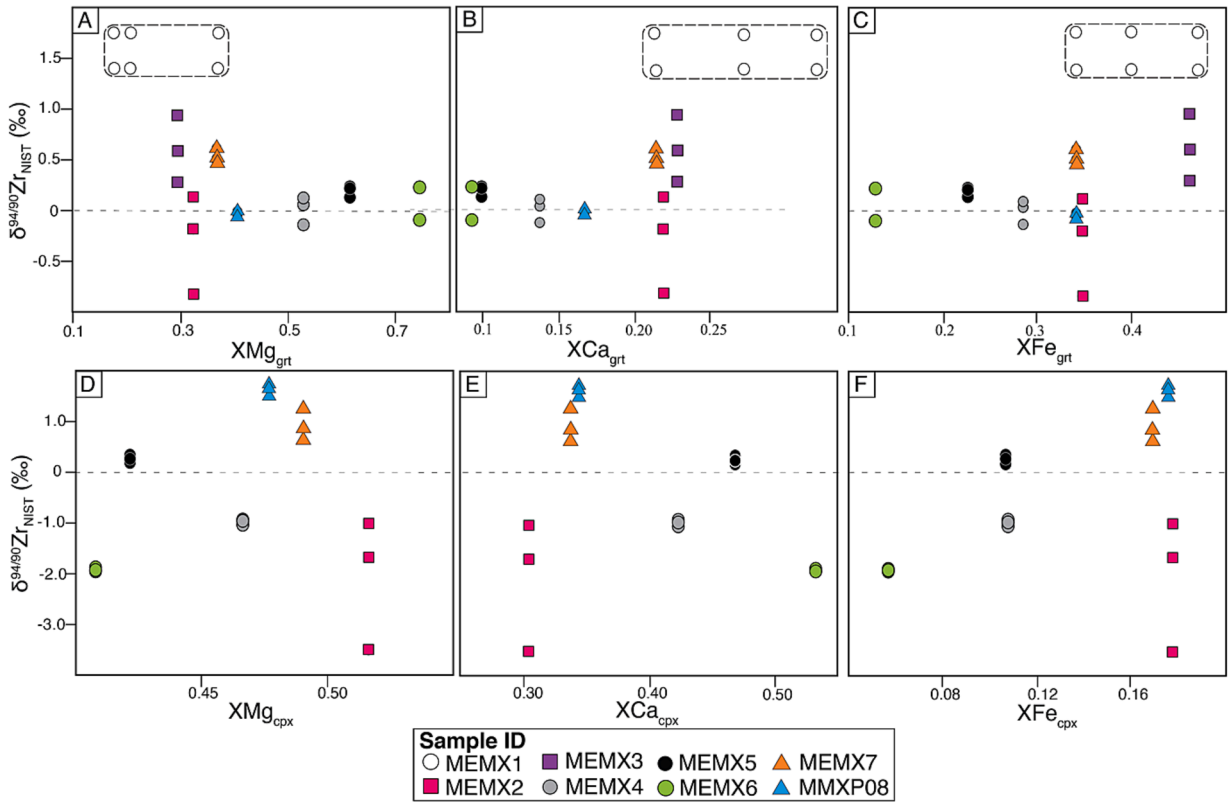

Fig. 7. Zirconium isotopic compositions of garnet and clinopyroxene mineral fractions vs. mineral chemistry expressed as mole fraction (X) of Ca, Mg, and Fe. Mineral chemistry from electron microprobe analyses by Bloch et al. (2017). Garnet in sample MEMX1 is chemically zoned so the field of analyzed grains is shown (dashed box).

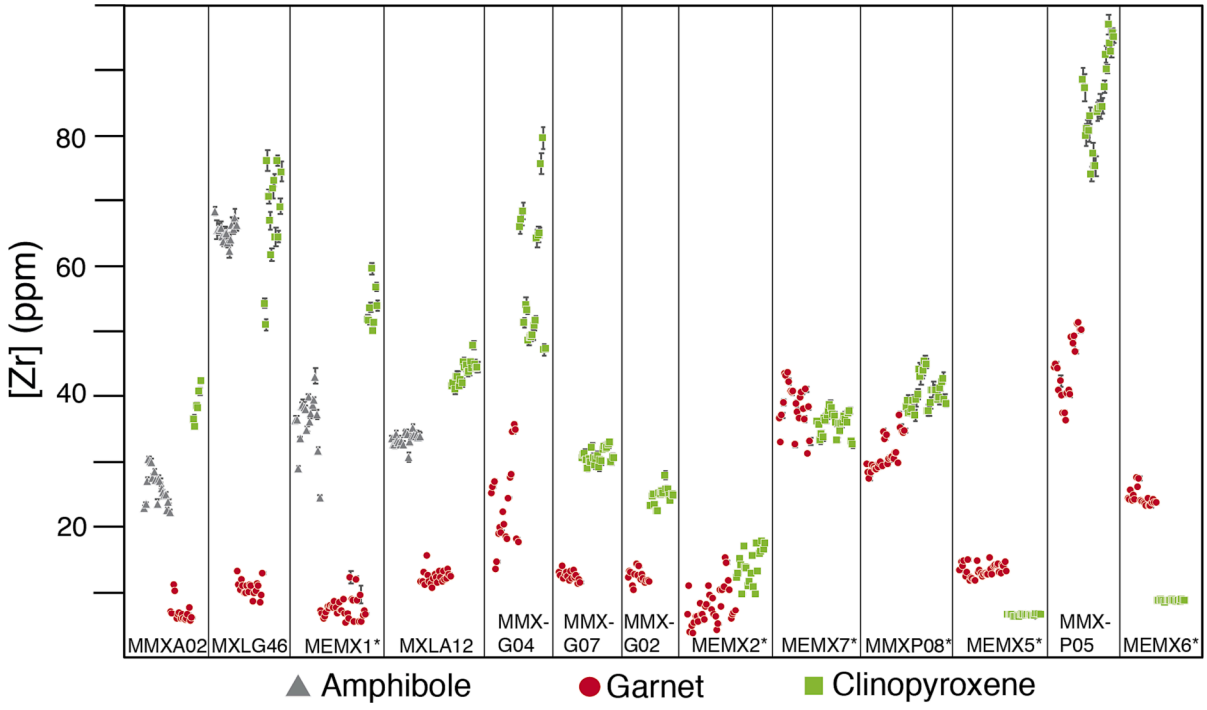

Fig. 8. *In situ* (LA-ICP-MS) Zr concentrations in rock-forming phases. Samples are in order (left to right) of increasing temperature from thermobarometry (Bloch et al., 2017; Zieman et al., 2023). Asterisks indicate samples analyzed for Zr isotopes within mineral fractions.

isotopic fractionation during calc-alkaline arc magma differentiation is limited and is thus unlikely to be a robust tracer of fractional crystallization.

4.2. Zr isotopic variability in the lower arc crust: A possible mechanism introducing $\delta^{94/90}$Zr heterogeneity into the mantle

Whereas the basaltic bombs and andesitic-dacitic volcanic rocks show very limited Zr isotope variability, the lower crust-derived cumulates have highly variable, although predominantly positive, $\delta^{94/90}$Zr values. The variability we observe in the whole rock (ultra)mafic cumulates does not correlate directly with differentiation indices (i.e., SiO_2 or Mg #; Fig. 3), temperature, or pressure (Fig. 9), and it remains unclear how this variability was induced (see discussion below). Regardless of the mechanisms causing these variations, this result has important implications for lower arc crust recycling. The Mercaderes (ultra)mafic xenoliths measured here represent the dense garnet-rich lower crust assemblages that have been widely hypothesized to recycle, or founder, into the mantle beneath continental arcs (Müntener and Ulmer, 2006; Müntener et al., 2001). Zieman et al. (2023) calculated densities for > 40 Mercaderes lower crustal cumulates and determined that the average density of the bulk arc root is ~0.1 g/cm^3 greater than the density of the underlying mantle. Thus, these lower crustal cumulates are expected to be density-unstable and ultimately recycle into the mantle. One of the garnet clinopyroxene xenoliths measured here (MEMX5; $\delta^{94/90}$Zr = +0.101 ± 0.012 ‰) was interpreted by Bloch et al. (2017) to represent a fragment of foundered lower arc crust based on its chemistry and high equilibrium pressure. Therefore, the Zr isotope variability measured in the cumulates has the potential to be introduced to the mantle *via* foundering. Additionally, Zr isotopic variability may be introduced to arc magmas— the pressure–temperature estimates for many of the cumulates indicate they equilibrated at conditions above the dry pyroxenite solidus (Bloch et al., 2017; Zieman et al., 2023), suggesting they may be partially melting in the lower crust and/or will melt as they founder into the hotter mantle wedge (e.g., Ducea et al., 2013; Elkins-Tanton, 2007). Thus, the $\delta^{94/90}$Zr variations we observe in arclogitic cumulates will need to be considered as a contributing variable to understand $\delta^{94/90}$Zr variations in arc magmas and sub-arc mantle rocks, which remain to be studied in detail for $\delta^{94/90}$Zr.

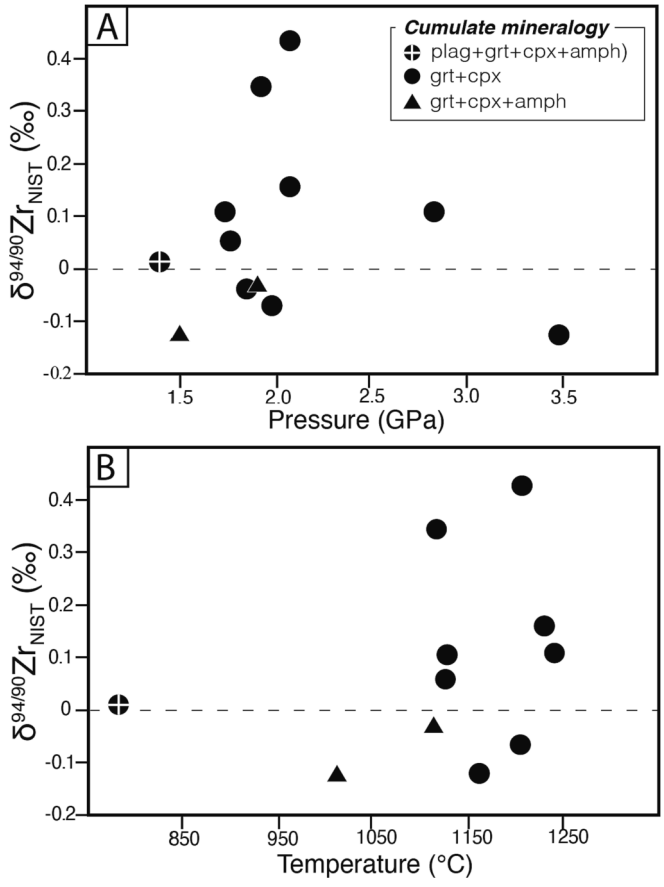

Fig. 9. Whole rock Zr isotopes of the Mercaderes cumulates vs. A) temperature and B) pressure.

4.3. Can the $\delta^{94/90}$Zr variations among rock-forming phases result from equilibrium partitioning?

To better understand the origin of the large $\delta^{94/90}$Zr variations observed between lower-crustal cumulates, and to test whether the Zr isotope variability amongst co-existing mineral fractions can be a result of equilibrium (vibrational) mass-dependent Zr isotope fractionation, we compare our measured $\delta^{94/90}$Zr values to theoretical predictions. Chen et al. (2020) obtained isotopic fractionation factors for several rock-forming mineral end-members using *ab initio* calculations. Among the phases they studied, of interest to our Mercaderes xenolithic cumulates are pyrope (representing garnet), diopside (clinopyroxene), tremolite (amphibole), and ilmenite. Reduced partition function (β) ratios of the phases of interest were used to calculate inter-mineral equilibrium fractionation coefficients (α) at relevant temperatures using the polynomial expansion coefficients for β presented by Chen et al. (2020). Isotopic fractionation coefficients between two phases 'A' and 'B', calculated as $\alpha_{A\text{-}B} = \beta_A/\beta_B$, are discussed through the text in 'big delta' notation, approximated as $\Delta^{94/90}Zr_{A\text{-}B} \approx 1000\ln\alpha_{A\text{-}B}$. For inter-mineral fractionations determined from our data and expressed in big delta, these were calculated as $\Delta^{94/90}Zr_{A\text{-}B} = \delta^{94}Zr/^{90}Zr_A - \delta^{94}Zr/^{90}Zr_B$. When expressing theoretical fractionations with respect to a melt, these are calculated using the β function for Ca-catapleiite (Fig. 10), which was used by Chen et al. (2020) as their melt proxy.

In the temperature range at which the cumulates equilibrated (782 °C–1293 °C; Bloch et al., 2017), diopside, tremolite, and pyrope in equilibrium with a melt are predicted to preferentially incorporate heavy Zr isotopes with a maximum $\Delta^{94/90}Zr \approx +0.25$ ‰ if Zr^{4+} substitutes for Si^{4+} in the tetrahedral site of any of these phases, and nearly an order of magnitude less if Zr^{4+} substitutes in the octahedral site instead (e.g., $\Delta^{94/90}Zr_{pyrope\text{-}melt} \sim +0.05$ ‰). Ilmenite on the other hand, is predicted to preferentially incorporate light Zr isotopes with respect to the melt, resulting in slightly negative $\Delta^{94/90}$Zr no larger in magnitude than −0.15 ‰ at the temperatures of interest. Therefore, vibrational equilibrium Zr isotope effects should produce limited fractionation between the mineral phases we measured at their conditions of equilibration, and therefore cannot be solely responsible for the large range of $\delta^{94/90}$Zr variability observed in the whole rock (ultra)mafic cumulates (-0.134 to 0.428 ‰). Furthermore, inter-mineral $\Delta^{94/90}$Zr driven by equilibrium fractionation should not exceed 0.4 ‰ in absolute magnitude even if the most extreme substitutions and β function from Chen et al. (2020) are used, yet co-existing garnet and amphibole fractions measured in this study have far greater inter-mineral variability with $\Delta^{94/90}Zr_{garnet\text{-}amphibole}$ up to 2.067 ‰ for sample MEMX1.

Equilibrium fractionation can be more specifically ruled out by comparing the measured $\Delta^{94/90}$Zr values from co-existing garnet-clinopyroxene and/or garnet-amphibole pairs to theoretical $\Delta^{94/90}$Zr values expected as a function of temperature. Fig. 11 shows binary plots in which the $\delta^{94/90}$Zr values of two minerals from a given sample are plotted with respect to one another. In this diagram, predicted equilibrium values can be plotted as lines of constant $\Delta^{94/90}$Zr for a given equilibration temperature. Zr isotopic fractionation for garnet-clinopyroxene and garnet-amphibole pairs at a given temperature are plotted for Zr substitutions involving both tetrahedral (4-fold, T) and octahedral (6-fold, M) crystallographic sites. The measured $\delta^{94/90}$Zr of co-existing mineral pairs in each sample are also plotted. Regardless of

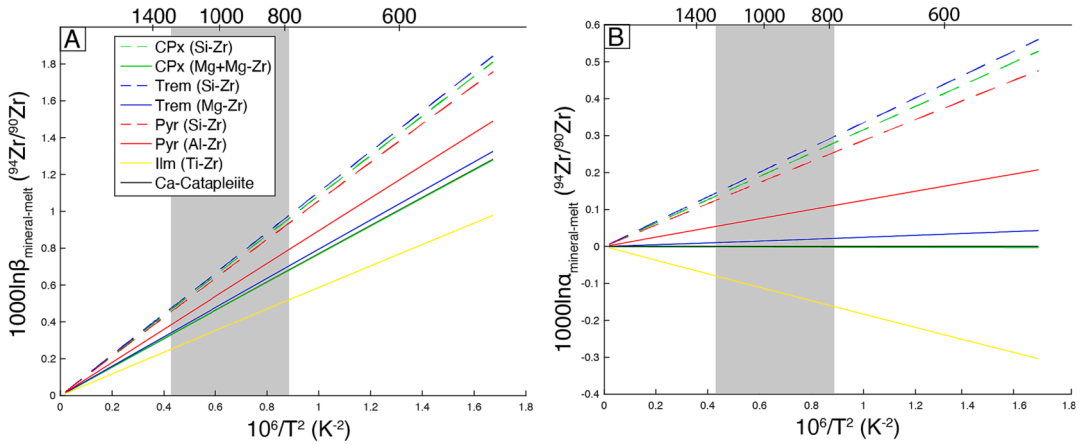

Fig. 10. A) Equilibrium (*ab initio*) reduced partition function ratios (1000lnβ) vs. temperature for Zr in clinopyroxene (diopside), garnet (pyrope), amphibole (tremolite), ilmenite, and Ca-catapleiite (a proxy for silicate melt), considering potential Zr substitutions in tetragonal and octahedral cation sites. Data from Chen et al. (2020). B) Equilibrium isotopic fractionation coefficient between mineral and melt ($1000\ln\alpha_{\text{mineral-melt}}$) vs. temperature. Gray field shows the temperature range of Mercaderes xenoliths analyzed in this study.

the site Zr occupies, all analyzed samples are evidently not in Zr isotopic equilibrium at the temperatures independently constrained from major-element equilibrium thermobarometry for each given sample (from Bloch et al., 2017). For example, for the measured $\delta^{94/90}$Zr value for amphibole in sample MEMX1 (panel E in Fig. 11), $\delta^{94/90}$Zr of co-existing garnet should not exceed ~−0.1 ‰ by equilibrium isotopic fractionation at the sample's temperature (1008 °C); however, co-existing garnet reaches +1.746 ‰. Thus, given all the above observations, we conclude that the large magnitudes of Zr isotopic fractionation observed at both the whole rock scale as well as between mineral fractions of the same rock, cannot be explained by equilibrium fractionation alone.

4.4. Kinetic Zr isotope fractionation in rock-forming phases

The magnitudes and directions of inter-mineral Zr isotope fractionation observed in this study are inconsistent with an equilibrium fractionation mechanism. Therefore, additional non-equilibrium processes must be at play. Although Zr diffusion has not been directly studied, high-field strength elements such as Hf are slow diffusing species in silicate minerals even at high temperature (Bloch and Ganguly, 2014; Bloch et al., 2020), implying that diffusive equilibrium (elemental and isotopic) amongst co-existing phases is difficult to achieve over short time scales. Although our lower crustal xenoliths resided at very high temperatures prior to eruption and are for the most part well equilibrated, faint to moderate major element zoning on garnets and pyroxenes has been observed in several of them (Bloch et al., 2017; Zieman et al., 2023), implying that perfect equilibrium was not achieved or was disrupted by a subsequent process. If this is true for major elements, then it must also be the case for Zr^{4+} which diffuses ~ 2 orders of magnitude slower than Mg^{2+} in garnet at similar temperatures using the diffusivity of Hf^{4+} in garnet from Bloch et al. (2015) as a proxy. Therefore, the distinct possibility that elemental Zr equilibrium throughout the samples was not achieved suggests that the concomitant diffusive fluxes that must be acting to equalize Zr chemical potential may be capable of imparting kinetic isotope fractionation effects, as has been found to be the case in other examples of Zr isotope distribution (e.g., Ibañez-Mejia and Tissot, 2019; Tompkins et al., 2023). The interpretation that Zr isotopic fractionation may be controlled by kinetic processes can be further supported by our *in situ* Zr concentration measurements using LA-ICP-MS, which demonstrate that Zr chemical equilibrium was not achieved even at these high temperatures (see next section).

Another way of showing that Zr concentrations in our measured mineral fractions do not reflect equilibrium Zr distributions is to evaluate our whole-rock and mineral data in binary mixing plots. If Zr elemental and isotopic concentrations were homogenous in a bi-mineralic garnet clinopyroxenite, the whole rock composition should plot as a two-component linear mixing line against Ca/Zr (Fig. 6), with the bulk rock falling between the garnet and clinopyroxene fractions (e.g., Fig. 4 of Johnson et al., 2019). This is because Ca is a homogenous major element in all three minerals of interest (garnet, clinopyroxene, and amphibole), but varies in concentration significantly between each mineral. In these plots, the $\delta^{94/90}$Zr and Ca/Zr ratios, which were measured from homogenized mixtures of dissolved grains of different sizes, must be affected by Zr isotopic and elemental zoning because: i) the $\delta^{94/90}$Zr of different aliquots of the same mineral from the same sample are in many cases different outside uncertainty; and ii) the Ca molar fractions of all fractions from the same mineral in the same sample are homogenous and consistent with electron microprobe chemistry (Fig. 4), yet different mineral fractions of the same phase from the same sample have variable Ca/Zr. In other words, the spread of Ca/Zr ratios in Fig. 6, and cases where garnet fractions (a relatively Ca-poor phase in our samples) have greater Ca/Zr ratios than clinopyroxene (a Ca-rich phase), is mostly controlled by the [Zr] of the dissolved phase (as opposed to [Ca]), which can be attributed to heterogeneous [Zr] distributions within each mineral phase.

Significant magnitudes of isotopic fractionation observed in other heavy stable isotope systems (e.g., Ca and Fe) are interpreted to result from non-equilibrium fractionation mechanisms at high temperature (e.g., Antonelli and Simon, 2020; Bai et al., 2019; Kang et al., 2020; Tian et al., 2020b; Xiao et al., 2016; Zhao et al., 2017). One well-documented non-equilibrium kinetic process is partial re-equilibration by chemical diffusion (e.g., Neukampf et al., 2020; Oeser et al., 2015; Richter et al., 2009; Sio et al., 2013; Sio et al., 2018). All the samples studied here equilibrated at sub-solidus conditions, so chemical diffusion along grain boundaries and/or volume diffusion within minerals are most relevant to the Mercaderes cumulates (i.e., because evaporation and Soret diffusion require the presence of vapors/liquids). For example, Kang et al. (2020) argues that Ca diffusion is responsible for Ca isotope fractionation in (ultra)mafic xenoliths from China. They suggest Ca diffusion can occur in the mantle during a change in pyroxene composition by percolating metasomatic melts, or by sub-solidus re-equilibration due to changing inter-mineral partition coefficients during changes in mantle temperature. In other words, because Ca partitioning between clinopyroxene and orthopyroxene is sensitive to changes in temperature (i.e., it is a geothermometer; Brey and Köhler, 1990), a change in temperature even in a chemically closed system introduces chemical potential gradients that drive sub-solidus, inter-mineral diffusive re-equilibration.

Zirconium isotopes have been shown to exhibit dramatic non-

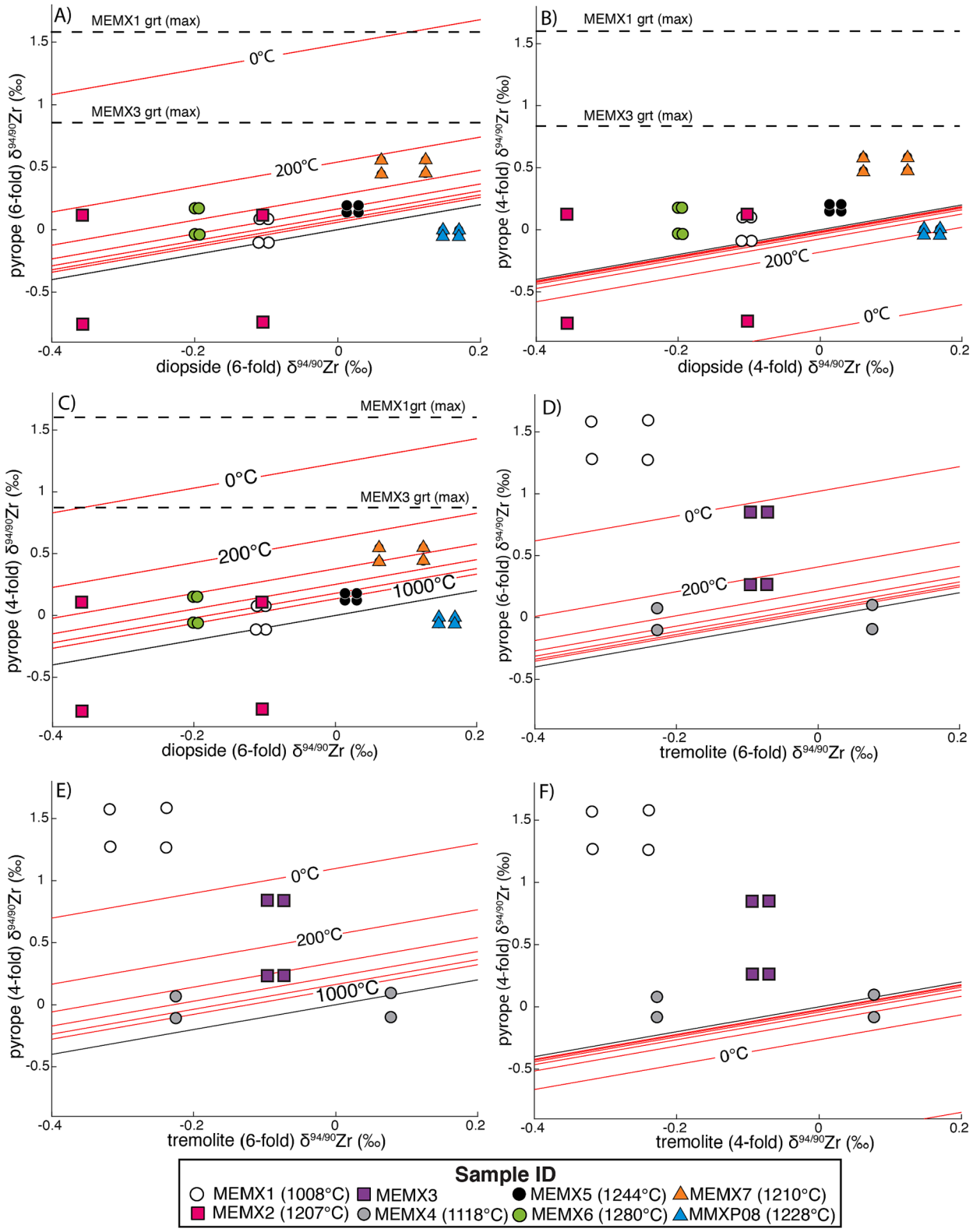

Fig. 11. Measured mineral fraction $\delta^{94/90}$Zr values compared to isothermal $\delta^{94/90}$Zr equilibrium (*ab initio*) predictions from Chen et al. (2020) for garnet, clinopyroxene, and amphibole end-members. Black line denotes the 1:1 line. Panels show different possible combinations of Zr substitutions in tetrahedral and octahedral crystallographic sites. Four points are plotted for each cumulate sample, showing the four possible combinations of maximum-minimum $\delta^{94/90}$Zr values of co-existing mineral fractions [e.g., four pink squares in panel A represent 1) max $\delta^{94/90}Zr_{grt}$ vs. max $\delta^{94/90}Zr_{cpx}$, 2) max $\delta^{94/90}Zr_{grt}$ vs. min $\delta^{94/90}Zr_{cpx}$, 3) min $\delta^{94/90}Zr_{grt}$ vs. max $\delta^{94/90}Zr_{cpx}$, and 4) min $\delta^{94/90}Zr_{grt}$ vs. min $\delta^{94/90}Zr_{cpx}$ for sample MEMX2]. Dashed lines in panels A-C show the maximum $\delta^{94/90}$Zr of garnet for the two samples from which clinopyroxene fractions were not recovered. (For interpretation of the references to colour in this figure legend, the reader is referred to the web version of this article.)

equilibrium kinetic effects in igneous environments involving crystallization from a melt (Ibañez-Mejia and Tissot, 2019; Méheut et al., 2021; Tissot and Ibañez-Mejia, 2021; Tompkins et al., 2023) but so far investigations have almost exclusively focused on zircon. In order to evaluate the possibility that changes in *P-T* conditions can be responsible for the inter-mineral $\Delta^{94/90}$Zr values we observe in these zircon-free rocks at sub-solidus conditions, one first needs to know the temperature dependence of the inter-mineral Zr partition coefficient (D_{Zr}) between the relevant phases. While the temperature dependence of Zr partitioning between clinopyroxene and orthopyroxene has been carefully determined for spinel-facies peridotites (Witt-Eickschen and O'Neill, 2005), partitioning between clinopyroxene, garnet, and amphibole for arclogitic bulk compositions at lower crustal conditions remain unknown. In the next section, we determine the temperature dependence of D_{Zr} between clinopyroxene and garnet, and use this relationship to evaluate the possibility that thermally-driven diffusive fluxes are capable of inducing kinetic isotope partitioning of Zr isotopes in our samples.

4.5. Temperature dependence of clinopyroxene-garnet Zr elemental partitioning in arclogites

Although we concluded that Zr stable isotopes are not directly related to absolute temperature or pressure (Fig. 9), it is possible that the change in temperature and/or pressure may induce fractionation via diffusive re-equilibration. We now consider how Zr stable isotopes may be fractionated by Zr diffusion due to temperature changes. *In situ* [Zr] measurements in adjacent clinopyroxene-garnet grains from a larger suite of samples from our same study locality were determined to calculate clinopyroxene-garnet partition coefficients ($D_{Zr}^{cpx/grt}$) for mineral assemblages and bulk compositions relevant to arclogites. We expanded the range of samples used for [Zr] measurements to cover a wider range of temperatures and have better leverage on the slope of the $\ln D_{Zr}$ vs. $1/T$ relationship. Reference temperatures for all samples studied for [Zr] are from Bloch et al. (2017) and Zieman et al. (2023).

Calculated $D_{Zr}^{cpx/grt}$ values for all studied samples are reported in Table 3 and plotted as a function of inverse temperature in Fig. 12. In general, Zr is more compatible in clinopyroxene than garnet ($D_{Zr}^{cpx/grt} > 1$), with the exception of our two highest-pressure (>2.8 GPa) garnet clinopyroxenites (MEMX5 and MEMX6). Measured clinopyroxene-garnet Zr partition coefficients ($D_{Zr}^{cpx/grt}$) indicate decreasing $D_{Zr}^{cpx/grt}$ with increasing temperature (Fig. 12a). This result is broadly consistent with the Zr partitioning trend observed by Griffin et al. (1988) for garnet-clinopyroxene pair inclusions in diamonds, though the *T* range of the samples studied by Griffin et al. (1988) is much narrower than the *T* range of our samples and the correlation between $D_{Zr}^{cpx/grt}$ and temperature in their diamond inclusions is weak. Performing a least-squares regression through the samples that share similar (lower lithospheric) pressures and ignoring the UHP pyroxenites, we obtain a temperature dependence for garnet-clinopyroxene Zr partitioning that can be expressed as $\ln D_{Zr}^{cpx/grt} = -5.7842\ (\pm 1.5665) + 9.2281\ (\pm 2.1069) * 1/T$ (K). The UHP pyroxenites yield $D_{Zr}^{cpx/grt}$ values that clearly deviate from the above regression, indicating either: i) that molar volume effects for the Zr substitution in one or both of these phases are important; and/or ii) that an additional crystal-chemical control on Zr substitution is at play. Although we do not observe a clear relationship between garnet or clinopyroxene composition with $\delta^{94/90}$Zr (Fig. 7), the garnets from the two UHP pyroxenites are significantly more pyrope-rich than the other samples (Fig. 12b). Although a crystal-chemical effect on Zr substitution is certainly possible, the two data points we obtained for the UHP pyroxenites are insufficient to draw general conclusions regarding the effects of mineral composition on Zr partitioning. Alternatively, one can evaluate the apparent pressure dependence on $D_{Zr}^{cpx/grt}$ by finding the partial molar volume change (ΔV°) of the exchange reaction that would bring the UHP pyroxenite $D_{Zr}^{cpx/grt}$ values to be in agreement with those of the lower pressure (lithospheric) arclogites. Using the relationship that describes the $D_{Zr}^{cpx/grt}$ of an exchange reaction on ΔV° (eq. 11.1.6 in Ganguly, 2020) we find that normalizing these two high-pressure samples to the average pressure of the samples used for the regression in Fig. 12 (i.e., 1.8 GPa) requires a partial molar volume change (ΔV°) of the reaction of 8.8 cm^3/mol. The ΔV° of garnet-clinopyroxene reaction involving substitution of Ca-Mg end members is on the order of 2 cm^3/mol (Mukhopadhyay, 1991), implying that the ΔV° of Zr substitution we calculate is reasonable, and thus pressure effects are a good candidate for the offset of $D_{Zr}^{cpx/grt}$ for MEMX5 and MEMX6.

Considering the decreasing $D_{Zr}^{cpx/grt}$ with increasing temperature determined from our samples, under sub-solidus conditions, Zr would be expected to diffuse from clinopyroxene into garnet during prograde (increasing temperature) thermal trajectories, while the opposite would be true during retrograde thermal paths. Thus, if the magnitude of diffusive isotope separation (i.e., β parameter of Richter et al., 1999) during volume diffusion of Zr in garnet and/or clinopyroxene is not negligible, then changes in temperature are likely to induce kinetic fractionation of Zr isotopes. In this scenario, the $\delta^{94/90}$Zr of coexisting minerals can potentially be used as kinetic monitors of prograde or retrograde thermal histories once the β parameters for the relevant phases are known.

Given the direction of $D_{Zr}^{cpx/grt}$ change we determined above as a function of temperature and assuming that lighter Zr isotopes diffuse faster than heavier ones (e.g., Richter et al., 1999; Watkins et al., 2017), we expect samples that have experienced cooling (retrograde paths) to have higher $\delta^{94/90}$Zr in garnet than in pyroxene beyond equilibrium values. This is because the increasing $D_{Zr}^{cpx/grt}$ values with decreasing temperature would result in a Zr diffusive flux going from garnet towards clinopyroxene accompanied by a more rapid transfer of lighter Zr isotopes. On the other hand, samples that have experienced heating (prograde paths) would be expected to display the opposite relation, with lower $\delta^{94/90}$Zr in garnet than in pyroxene, beyond expected equilibrium values.

Despite the clear expectations imposed by our new $\ln D_{Zr}$ vs. 1/T trend, the implications for $\delta^{94/90}$Zr are difficult to test with our samples. This is because the relatively rapid major element diffusion in the high-temperature lower-lithospheric setting we studied results in major element chemical profiles that are in general well equilibrated, and thus prograde or retrograde histories are difficult –if not impossible– to resolve given the accuracy/precision of existing geothermobarometers (Bloch et al., 2017; Zieman et al., 2023). Combined temperature–time and Zr isotope studies in mineral fractions from other geologic environments will be needed to fully test this hypothesis.

We note that the natural partitioning results for our high-pressure samples are in relatively good agreement with mineral-melt partitioning results from 2.5 GPa experiments by Green et al. (1989) where

Table 3
Zirconium clinopyroxene-garnet partition coefficients.

Sample ID	T* (°C)	1000/T (1000/K)	P* (GPa)	$\ln(D)Zr_{cpx/grt}$	2se
MMXA02	782	0.95	1.39	2.12	*0.06*
MXLG46	919	0.84	1.40	2.03	*0.06*
MEMX1	1008	0.78	1.47	2.18	*0.45*
MXLA12	1021	0.77	1.66	1.39	*0.03*
MMXG04	1115	0.72	1.92	1.01	*0.11*
MMXG07	1126	0.71	1.76	1.04	*0.04*
MMXG02	1128	0.71	1.27	0.73	*0.08*
MEMX2	1207	0.68	1.98	0.79	*0.14*
MEMX7	1210	0.67	2.08	−0.08	*0.04*
MMXP08	1228	0.67	2.08	0.26	*0.04*
MEMX5	1244	0.66	2.84	−0.96	*0.04*
MMXP05	1253	0.66	1.85	0.70	*0.04*
MEMX6	1280	0.64	4.22	−1.16	*0.04*

* Temperature and pressures from Bloch et al. (2017) and Zieman et al. (2023) except for the P-T of MEMX1, determined for this publication after the methods of Zieman et al. (2023).

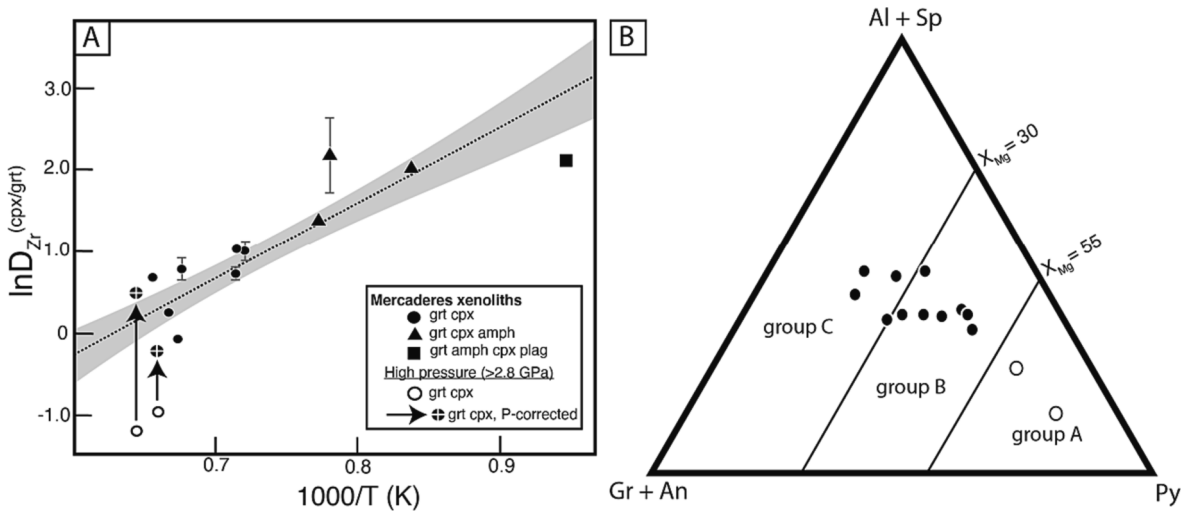

Fig. 12. A) Partition coefficient of Zr between clinopyroxene and garnet as a function of temperature. Gray field indicates the 2 SD uncertainty envelope, calculated after Browaeys (2021). B) Average garnet composition for each xenolith in panel A (Bloch et al., 2017; Zieman et al., 2023), plotted on an end-member ternary diagram after Coleman et al. (1965). Al—almandine. An—andradite. Sp—spessartine. Gr—Grossular. Py—Pyrope.

garnet and clinopyroxene are in equilibrium with highly hydrous basaltic liquids. Green et al. (1989) find that Zr is moderately incompatible in garnet (D ~ 0.7) and more incompatible in clinopyroxene (D ~ 0.1) at 2.5 GPa and 1100 °C, yielding a $D_{Zr}^{cpx/grt}$ of ~0.14 ± 0.07, which is close to the results from our two high-pressure natural samples ($D_{Zr}^{cpx/grt}$ = 0.31–0.38 ± 0.10; Fig. S2). The $\ln D_{Zr}^{cpx/grt}$ of our high-pressure xenoliths also plot in the general range of the garnet and clinopyroxene inclusions in diamonds from West Australia (Griffin et al., 1988; see Fig. S2), which also equilibrated at UHP conditions (~5 GPa). Thus, clinopyroxene-garnet Zr partitioning may indeed have a significant pressure-dependence, which would also impact the isotopic fractionation through the effects that concurrent pressure and temperature changes may have in the direction of Zr diffusive re-equilibration. For both the Mercaderes high-pressure samples and the diamond inclusions, $D_{Zr}^{cpx/grt}$ decreases with increasing pressure; therefore, increasing pressure should have the same effect on Zr isotopes as increasing temperature, lowering $\delta^{94/90}$Zr in garnet relative to pyroxene.

In summary, several parameters can influence the direction and magnitude of Zr exchange reactions between garnet and clinopyroxene and thus control the magnitude of kinetic isotopic fractionation. However, key parameters that are critical to quantify these reactions under sub-solidus conditions, such as Zr diffusivities in rock-forming phases and diffusion β coefficients, remain unknown. Future experiments that can control for bulk rock composition, temperature, and pressure are needed to better constrain Zr partitioning in arclogite rock-forming phases at lower lithospheric and upper mantle conditions, as well as quantify the effects that changing *P* and *T* conditions can have on $\delta^{94/90}$Zr. Water content should also be considered, as H_2O is known to affect HFSE partitioning in olivine (e.g., Witt-Eickschen and O'Neill, 2005 and references therein). Future work is also necessary to resolve which crystal sites Zr occupies in garnet, clinopyroxene, and amphibole, as well as Zr diffusion rates and mechanisms in these phases.

Altogether, these data will not only help further explain the variability observed in arclogite cumulates, but can also potentially be applied to determining cooling or heating rates in high-temperature systems, given the observation that $\delta^{94/90}$Zr in our samples are recording kinetic process(es) governed by the temperature dependency of mineral–mineral Zr partition coefficients under lower arc crust conditions. Thus, Zr stable isotopes have the potential to elucidate metamorphic processes in the continental lower arc crust, which has broad implications for continental crust formation in continental arc settings. Additionally, Zr stable isotopes may be ultimately applicable to deconvolve the metamorphic histories of garnet-bearing mantle pyroxenites (i.e., recycled eclogites vs. arclogites). For instance, two samples in this study equilibrated at mantle depths (MEMX5 and MEMX6) so constraining their origins and thermal histories using Zr stable isotopes would help elucidate lower crustal recycling and/or mantle metasomatism once the temperature- and pressure-dependence of Zr isotope fractionation are better quantified.

5. Conclusions

Zirconium stable isotope variability is limited in primitive calc-alkaline arc magmas and evolved volcanic rocks from the NVZ, suggesting Zr stable isotope fractionation is not a useful magmatic differentiation tracer in continental arc settings. The evolved volcanic rocks have slightly higher $\delta^{94/90}$Zr than their mafic counterparts, which may be attributed to crystallization of isotopically light ilmenite during differentiation as these volcanic samples remained unsaturated with respect to zircon. Garnet clinopyroxenite cumulates derived from the lower arc crust have highly variable $\delta^{94/90}$Zr, but this variability is not directly related to their absolute temperature and/or pressure, or composition.

Zirconium isotopic measurements of garnet, clinopyroxene, and amphibole mineral fractions from lower crust-derived cumulates revealed very large magnitudes for inter-mineral $\Delta^{94/90}$Zr, in excess of 2 ‰, with garnet being predominantly heavy relative to co-existing clinopyroxene and amphibole. This isotopic variability cannot be driven solely by equilibrium fractionation, but rather requires a kinetic process. Incomplete diffusive re-equilibration of Zr at sub-solidus conditions driven by changing $D_{Zr}^{cpx/grt}$ values as a function of temperature and possibly also pressure, water content, and crystal chemistry may be controlling diffusive Zr isotopic fractionation between rock-forming minerals. Full quantification of these fractionations, however, requires further research about Zr partitioning, diffusion kinetics (elemental and isotopic), and coordination in rock-forming minerals. We observe, however, that once the relevant kinetic parameters for Zr diffusive isotope fractionation are quantified, $\delta^{94/90}$Zr variations among co-existing phases can be used to recover the rates of cooling or heating (i.e., a geospeedometer) in high-temperature igneous and metamorphic environments.

The high pressure cumulates studied here directly sample the density-unstable section of the lower Andean crust expected to recycle into the mantle via lower crustal foundering. Thus, because their $\delta^{94/90}$Zr values are highly variable, we conclude that lower crustal foundering in subduction zones can be an important mechanism introducing

mass-dependent Zr isotope variability into the mantle. The large variations in $\delta^{94/90}$Zr observed in our arclogites can become an useful tool to trace the origins of mantle pyroxenites, and underscore the need for more detailed studies of $\delta^{94/90}$Zr focusing on understanding the composition (and possible variations) of Earth's upper and lower mantle.

Declaration of competing interest

The authors declare that they have no known competing financial interests or personal relationships that could have appeared to influence the work reported in this paper.

Acknowledgements

This work was supported by NSF-EAR grants 2131632 and 2143168 (to MIM), and 1824002 (to FLHT). FLHT acknowledges additional support from NSF grant MGG-2054892, a Packard Fellowship, a research award from the Heritage Medical Research Institute, and startup funds from Caltech.

Data availability

Data are available through Mendeley Data at https://data.mendeley.com/datasets/v829hs8953/1.

Appendix A. Supplementary material

The supplementary material includes Table S1, which contains whole rock major element geochemistry for the Mercaderes and Doña Juana samples, as well as two figures. Fig. S1 presents the results of rhyolite-MELTS calculations coupled to a zircon saturation parameterization, showing that zircon did not saturate in the felsic volcanic rocks studied here. Fig. S2 is modified from Fig. 12 to include literature data of clinopyroxene-garnet partition coefficients. Supplementary material to this article can be found online at https://doi.org/10.1016/j.gca.2023.11.023.

References

Akram, W., Schönbächler, M., 2016. Zirconium isotope constraints on the composition of Theia and current Moon-forming theories. Earth Planet. Sci. Lett. 449, 302–310.
Antonelli, M.A., Simon, J.I., 2020. Calcium isotopes in high-temperature terrestrial processes. Chem. Geol. 548.
Bai, Y., Su, B.-X., Xiao, Y., Chen, C., Cui, M.-M., He, X.-Q., Qin, L.-P., Charlier, B., 2019. Diffusion-driven chromium isotope fractionation in ultramafic cumulate minerals: elemental and isotopic evidence from the Stillwater Complex. Geochim. Cosmochim. Acta. 263, 167–181.
Baker, M.B., Grove, T.L., Price, R., 1994. Primitive basalts and andesites from the Mt. Shasta region, N. California: products of varying melt fraction and water content. Contrib. Mineral. Petrol. 118, 111–129.
Bloch, E., Ganguly, J., 2014. ^{176}Lu–^{176}Hf and ^{147}Sm–^{143}Nd ages of the Martian shergottites: evaluation of the shock-resetting hypothesis through diffusion kinetic experiments and modeling, and petrological observations. Earth Planet. Sci. Lett. 395, 173–183.
Bloch, E., Ganguly, J., Hervig, R., Cheng, W., 2015. ^{176}Lu–^{176}Hf geochronology of garnet I: experimental determination of the diffusion kinetics of Lu^{3+} and Hf^{4+} in garnet, closure temperatures and geochronological implications. Contrib. Mineral. Petrol. 169 (12).
Bloch, E., Ibañez-Mejia, M., Murray, K., Vervoort, J., Müntener, O., 2017. Recent crustal foundering in the Northern Volcanic Zone of the Andean arc: petrological insights from the roots of a modern subduction zone. Earth Planet. Sci. Lett. 476, 47–58.
Bloch, E.M., Jollands, M.C., Devoir, A., Bouvier, A.S., Ibañez-Mejia, M., Baumgartner, L. P., 2020. Multispecies diffusion of yttrium, rare earth elements and hafnium in garnet. J. Petrol. 61 (7), egaa055.
Brey, G.P., Köhler, T., 1990. Geothermobarometry in four-phase lherzolites II. New thermobarometers, and practical assessment of existing thermobarometers. J. Petrol. 31, 1353–1378.
Browaeys, J., 2021. Linear fit with both uncertainties in x and y. MATLAB Central File Exchange.
Bryant, J.A., Yogodzinski, G.M., Hall, M.L., Lewicki, J.L., Bailey, D.G., 2006. Geochemical constraints on the origins of volcanic rocks from the Andean Northern Volcanic Zone. Ecuador. J. Petrol. 47 (6), 1147–1175.
Chen, X., Wang, W., Zhang, Z., Nie, N.X., Dauphas, N., 2020. Evidence from Ab initio and transport modeling for diffusion-driven zirconium isotopic fractionation in igneous rocks. ACS Earth Space Chem. 4, 1572–1595.
Chiaradia, M., Müntener, O., Beate, B., Fontignie, D., 2009. Adakite-like volcanism of Ecuador: lower crust magmatic evolution and recycling. Contrib. Mineral. Petrol. 158, 563–588.
Coleman, R.G., Lee, D.E., Beatty, L.B., Brannock, W.W., 1965. Eclogites and eclogites: their differences and similarities. Geol. Soc. Am. Bull. 76, 483–508.
Deng, Z., Chaussidon, M., Savage, P., Robert, F., Pik, R., Moynier, F., 2019. Titanium isotopes as a tracer for the plume or island arc affinity of felsic rocks. Proc. Natl. Acad. Sci. 116, 1132–1135.
Ducea, M.N., Seclaman, A.C., Murray, K.E., Jianu, D., Schoenbohm, L.M., 2013. Mantle-drip magmatism beneath the Altiplano-Puna plateau, central Andes. Geology 41, 915–918.
Elkins-Tanton, L.T., 2007. Continental magmatism, volatile recycling, and a heterogeneous mantle caused by lithospheric gravitational instabilities. J. Geophys. Res. 112.
Ganguly, J., 2020. Thermodynamics in Earth and Planetary Sciences, 2nd ed. Springer Nature Switzerland, Switzerland.
Greber, N.D., Dauphas, N., Bekker, A., Ptáček, M.P., Bindeman, I.N., Hofmann, A., 2017. Titanium isotopic evidence for felsic crust and plate tectonics 3.5 billion years ago. Science 357, 1271–1274.
Green, T.H., Sie, S.H., Ryan, C.G., Cousens, D.R., 1989. Proton microprobe-determined partitioning of Nb, Ra, Zr, Sr, and Y between garnet, clinopyroxene, and basaltic magma at high pressure and temperature. Chem. Geol. 74, 201–216.
Griffin, W.L., Jaquesz, A.L., Sie, S.H., Ryan, C.G., Cousens, D.R., Suter, G.F., 1988. Conditions of diamond growth: a proton microprobe study of inclusions in West Australian diamonds. Contrib. Mineral. Petrol. 99, 143–158.
Guo, J.L., Wang, Z., Zhang, W., Moynier, F., Cui, D., Hu, Z., Ducea, M.N., 2020. Significant Zr isotope variations in single zircon grains recording magma evolution history. Proc. Natl. Acad. Sci. 117, 21125–21131.
Guo, J.-L., Wang, Z., Zhang, W., Feng, L., Moynier, F., Hu, Z., Zhou, L., Liu, Y., 2023. Zirconium and its stable isotopes in igneous systems. Earth-Sci. Rev. 237.
Hoare, L., Klaver, M., Saji, N.S., Gillies, J., Parkinson, I.J., Lissenberg, C.J., Millet, M.-A., 2020. Melt chemistry and redox conditions control titanium isotope fractionation during magmatic differentiation. Geochim. Cosmochim. Acta 282, 38–54.
Ibañez-Mejia, M., Tissot, F.L.H., 2019. Extreme Zr stable isotope fractionation during magmatic fractional crystallization. Sci. Adv. 5 (12), eaax8648.
Inglis, E.C., Creech, J.B., Deng, Z., Moynier, F., 2018. High-precision zirconium stable isotope measurements of geological reference materials as measured by double-spike MC-ICPMS. Chem. Geol. 493, 544–552.
Inglis, E.C., Moynier, F., Creech, J., Deng, Z., Day, J.M.D., Teng, F.-Z., Bizzarro, M., Jackson, M., Savage, P., 2019. Isotopic fractionation of zirconium during magmatic differentiation and the stable isotope composition of the silicate Earth. Geochim. Cosmochim. Acta 250, 311–323.
Jagoutz, O.E., 2010. Construction of the granitoid crust of an island arc. Part II: a quantitative petrogenetic model. Contrib. Mineral. Petrol. 160, 359–381.
Johnson, A.C., Aarons, S.M., Dauphas, N., Nie, N.X., Zeng, H., Helz, R.T., Romaniello, S. J., Anbar, A.D., 2019. Titanium isotopic fractionation in Kilauea Iki lava lake driven by oxide crystallization. Geochim. Cosmochim. Acta 264, 180–190.
Johnson, A.C., Zhang, Z.J., Dauphas, N., Rudnick, R.L., Foden, J.D., Toc, M., 2023. Redox and mineral controls on Fe and Ti isotopic fractionations during calc-alkaline magmatic differentiation. Geochim. Cosmochim. Acta 355, 1–12.
Kang, J.-T., Zhou, C., Huang, J.-Y., Hao, Y.-T., Liu, F., Zhu, H.-L., Zhang, Z.-F., Huang, F., 2020. Diffusion-driven Ca-Fe isotope fractionations in the upper mantle: implications for mantle cooling and melt infiltration. Geochim. Cosmochim. Acta 290, 41–58.
Klaver, M., MacLennan, S.A., Ibañez-Mejia, M., Tissot, F.L.H., Vroon, P.Z., Millet, M.-A., 2021. Reliability of detrital marine sediments as proxy for continental crust composition: the effects of hydrodynamic sorting on Ti and Zr isotope systematics. Geochim. Cosmochimica Cosmochim. Acta 310, 221–239.
Klemme, S., Günther, D., Hametner, K., Prowatke, S., Zack, T., 2006. The partitioning of trace elements between ilmenite, ulvospinel, armalcolite and silicate melts with implications for the early differentiation of the moon. Chem. Geol. 234, 251–263.
Lee, C.T.A., 2014. Physics and Chemistry of Deep Continental Crust Recycling. In: Holland, H.D., Turekian, K.K. (Eds.), Treatise on Geochemistry. Elsevier Ltd., pp. 423–456
Lee, C.-T.-A., Cheng, X., Horodyskyj, U., 2006. The development and refinement of continental arcs by primary basaltic magmatism, garnet pyroxenite accumulation, basaltic recharge and delamination: insights from the Sierra Nevada. California. Contrib. Mineral. Petrol. 151, 222–242.
Lee, C.-T.-A., Morton, D.M., Kistler, R.W., Baird, A.K., 2007. Petrology and tectonics of Phanerozoic continent formation: From island arcs to accretion and continental arc magmatism. Earth Planet. Sci. Lett. 263, 370–387.
Méheut, M., Ibañez-Mejia, M., Tissot, F.L.H., 2021. Drivers of zirconium isotope fractionation in Zr-bearing phases and melts: The roles of vibrational, nuclear field shift and diffusive effects. Geochim. Cosmochim. Acta 292, 217–234.
Millet, M.-A., Dauphas, N., Greber, N.D., Burton, K.W., Dale, C.W., Debret, B., Macpherson, C.G., Nowell, G.M., Williams, H.M., 2016. Titanium stable isotope investigation of magmatic processes on the Earth and Moon. Earth Planet. Sci. Lett. 449, 197–205.
Mukhopadhyay, B., 1991. Garnet-clinopyroxene geobarometry: the problems, a prospect, and an approximate solution with some applications. Am. Mineral. 76, 512–529.
Münker, C., Wörner, G., Yogodzinski, G., Churikova, T., 2004. Behaviour of high field strength elements in subduction zones: constraints from Kamchatka-Aleutian arc lavas. Earth and Planet. Sci. Lett. 224, 275–293.

Müntener, O., Ulmer, P., 2006. Experimentally derived high-pressure cumulates from hydrous arc magmas and consequences for the seismic velocity structure of lower arc crust. Geophys. Res. Lett. 33.
Müntener, O., Ulmer, P., 2018. Arc crust formation and differentiation constrained by experimental petrology. Am. J. Sci. 318, 64–89.
Müntener, O., Kelemen, P.B., Grove, T.L., 2001. The role of H_2O during crystallization of primitive arc magmas under uppermost mantle conditions and genesis of igneous pyroxenites: an experimental study. Contrib. Mineral. Petrol. 141, 643–658.
Neukampf, J., Ellis, B.S., Laurent, O., Steinmann, L.K., Ubide, T., Oeser, M., Magna, T., Weyer, S., Bachmann, O., 2020. Time scales of syneruptive volatile loss in silicic magmas quantified by Li isotopes. Geology 49, 125–129.
Oeser, M., Dohmen, R., Horn, I., Schuth, S., Weyer, S., 2015. Processes and time scales of magmatic evolution as revealed by Fe-Mg chemical and isotopic zoning in natural olivines. Geochim. Cosmochim. Acta 154, 130–150.
Pardo, N., Pulgarín, B., Betancourt, V., Lucchi, F., Valencia, L.J., 2019. Facing geological mapping at low-latitude volcanoes: the Doña Juana Volcanic Complex study-case, SW-Colombia. J. Volcanol. Geotherm. Res. 385, 46–67.
Richter, F.M., Liang, Y., Davis, A.M., 1999. Isotope fractionation by diffusion in molten oxides. Geochim. Cosmochim. Acta 63, 2853–2861.
Richter, F.M., Dauphas, N., Teng, F.-Z., 2009. Non-traditional fractionation of non-traditional isotopes: evaporation, chemical diffusion and Soret diffusion. Chem. Geol. 258, 92–103.
Rodriguez-Vargas, A., Koester, E., Mallmann, G., Conceição, R.V., Kawashita, K., Weber, M.B.I., 2005. Mantle diversity beneath the Colombian Andes, Northern Volcanic Zone: Constraints from Sr and Nd isotopes. Lithos 82, 471–484.
Saji, N.S., Rudnick, R.L., Gaschnig, R.M., Millet, M.-A., 2023. Titanium isotope evidence for the high topography of Nuna and Gondwana - Implications for Earth's redox and biological evolution. Earth Planet. Sci. Lett. 615, 118214.
Schönbächler, M., Rehkämper, M., Halliday, A.N., Lee, D.-C., Bourot-Denise, M., Zanda, B., Hattendorf, B., Günther, D., 2002. Niobium-zirconium chronometry and early solar system development. Science 295.
Sio, C.K.I., Dauphas, N., Teng, F.-Z., Chaussidon, M., Helz, R.T., Roskosz, M., 2013. Discerning crystal growth from diffusion profile in zoned olivine by *in situ* Mg-Fe isotope analyses. Geochim. Cosmochim. Act 123, 302–321.
Sio, C.K., Roskosz, M., Dauphas, N., Bennett, N.R., Mock, T., Shahar, A., 2018. The isotope effect for Mg-Fe interdiffusion on olivine and its dependence on crystal orientation, composition, and temperature. Geochim. Cosmochim. Acta 239, 463–480.
Syracuse, E.M., Maceira, M., Prieto, G.A.., Zhang, H., Ammon, 2016. Multiple plates subducting beneath Colombia, as illuminated by seismicity and velocity from joint inversion seismic and gravity data. Earth Planet. Sci. Lett. 444, 139–149.
Tian, S., Inglis, E.C., Creech, J.B., Zhang, W., Wang, Z., Hu, Z., Liu, Y., Moynier, F., 2020a. The zirconium stable isotope compositions of 22 geological reference materials, 4 zircons and 3 standard solutions. Chem. Geol. 555, 119791.
Tian, H.-C., Zhang, C., Teng, F.-Z., Long, Y.-J., Li, S.-G., He, Y., Ke, S., Chen, X.-Y., Yang, W., 2020b. Diffusion-driven extreme Mg and Fe isotope fractionation in Panzhihue ilmenite: implications for the origin of mafic intrusion. Geochim. Cosmochim. Acta. 278, 361–375.
Tissot, F.L.H., Ibañez-Mejia, M., 2021. Unlocking the single-crystal record of heavy stable isotopes. Elements 17, 389–394.
Tissot, F.L.H., Ibañez-Mejia, M., Rabb, S.A., Kraft, R.A., Vocke, R.B., Fehr, M.A., Schönbächler, M., Tang, H., Young, E.D., 2023. A community-led calibration of Zr isotope reference materials: NIST candidate RM 8299 and SRM 3169. J. Anal. at. Spectrom. 38, 2087–2104.
Tompkins, H.G.D., Zieman, L.J., Ibañez-Mejia, M., Tissot, F.L.H., 2020. Zirconium stable isotope analysis of zircon by MC-ICP-MS: methods and application to evaluating intra-crystalline zonation in a zircon megacryst. J. Anal. at. Spectrom. 35 (6), 1167–1186.
Tompkins, H.G.D., Ibañez-Mejia, M., Tissot, F.L.H., Bloch, E., Wang, Y., Trail, D., 2023. Zircon growth experiments reveal limited equilibrium Zr isotope fractionation in magmas. Geochem. Perspect. Lett. 25, 25–29.
Watkins, J.M., DePaolo, D.J., Watson, E.B., 2017. Kinetic fractionation of non-traditional stable isotopes by diffusion and crystal growth reactions. Rev. Mineral. Geochem. 82, 85–125.
Weber, M.B.I., Tarney, J., Kempton, P.B., Kent, R.W., 2002. Crustal make-up of the northern Andes: evidence based on deep crustal xenolith suites, Mercaderes, SW Colombia. Tectonophysics 345, 49–82.
Weyer, S., Munkera, C., Mezgera, K., 2003. Nb/Ta, Zr/Hf and REE in the depleted mantle: implications for the differentiation history of the crust-mantle system. Earth Planet. Sci. Lett. 205, 309–324.
Witt-Eickschen, G., O'Neill, H.S.C., 2005. The effect of temperature on the equilibrium distribution of trace elements between clinopyroxene, orthopyroxene, olivine and spinel in upper mantle peridotite. Chem. Geol. 221, 65–101.
Xiao, Y., Teng, F.-Z., Su, B.-X., Hu, Y., Zhou, M.-F., Zhu, B., Shi, R.-D., Huang, X.-H., He, Y.-S., 2016. Iron and magnesium isotopic constraints on the origina of chemical heterogeneity in podiform chromitite from the Luobusa ophiolite, Tibet. Geochem. Geophys. Geosys. 17, 940–953.
Yuan, Y., Guo, J.-L., Zong, K., Feng, L., Wang, Z., Moynier, F., Zhang, W., Hu, Z., Xu, H., 2022. Stable zirconium isotopic fractionation during alkaline magma differentiation: implications for the differentiation of continental crust. Geochim. Cosmochim. Acta 326, 41–55.
Zhao, X., Zhang, Z., Huang, S., Liu, Y., Li, X., Zhang, H., 2017. Coupled extremely light Ca and Fe isotopes in peridotites. Geochim. Cosmochim. Act 208, 368–380.
Zieman, L., Ibañez-Mejia, M., Rooney, A.D., Bloch, E., Pardo, N., Schoene, B., Szymanowski, D., 2023. To sink, or not to sink: The thermal and density structure of the modern northern Andean arc constrained by xenolith petrology. Geology 51, 586–590.